

Triggered aseismic fault slip from nearby earthquakes, static or dynamic effect?

Wen-xuan Du,^{1,2} Lynn R. Sykes,^{1,2} Bruce E. Shaw,^{1,2} and Christopher H. Scholz^{1,2}

Received 4 June 2002; revised 20 September 2002; accepted 25 October 2002; published 28 February 2003.

[1] Observations show that an earthquake can affect aseismic slip behavior of nearby faults and produce “triggered aseismic fault slip.” Two types of stress changes are often examined by researchers as possible triggering sources. One is the static stress change associated with the faulting process and the other is the dynamic stress change or transient deformation generated by the passage of seismic waves. No consensus has been reached, however, regarding the mechanism(s) of triggered aseismic fault slip. We evaluate the possible triggering role of static stress changes by examining observations made after 10 large earthquakes in California. Most of the nearby fault segments that slipped aseismically were encouraged to move by the imposed positive changes in static Coulomb Failure Stress (CFS). Nonetheless, three discrepancies or failures with this model exist, which implies that static stress triggering either is or is not the sole mechanism causing the observed triggered slip. We then use a spring-slider system as a simplified fault model to study its slip behavior and the impact of transient (dynamic) loading on it. We show that a two-state-variable rate-dependent and state-dependent frictional law can generate creep events. Transient loads are then put into the system. Certain types of them can cause a large time advance of (or trigger) the next creep event. While our work examines triggered creep events near the surface, it may well have implications for the occurrence of similar events near the bottom of the seismogenic zone where a transition in frictional stability occurs. *INDEX TERMS*: 7209 Seismology: Earthquake dynamics and mechanics; 7260 Seismology: Theory and modeling; 8168 Tectonophysics: Evolution of the Earth: Stresses—general

Citation: Du, W.-x., L. R. Sykes, B. E. Shaw, and C. H. Scholz, Triggered aseismic fault slip from nearby earthquakes, static or dynamic effect?, *J. Geophys. Res.*, 108(B2), 2131, doi:10.1029/2002JB002008, 2003.

1. Introduction

[2] Slip on certain faults can take place in both seismic and aseismic ways, resulting in either the occurrence of earthquakes or fault creep. Fault creep, which is also called stable aseismic fault slip, was first observed in the 1960s on a segment of the San Andreas fault in central California [Steinbrugge and Zacher, 1960; Tocher, 1960]. Later this phenomenon was also found along the Hayward fault and the southern part of the Calaveras fault in the San Francisco Bay area and several other fault segments in southern California [Nason, 1971; Gouly and Gilman, 1978; Schulz et al., 1982; Louie et al., 1985; Sylvester, 1986]. Fault creep may occur gradually over a long period of time (secular creep), or it may take place as episodes of displacement (creep events).

[3] When a fault slips seismically and generates an earthquake, not only are the average values of shear stress on it reduced, but also the shear and normal stresses in the

surrounding area are altered. Recent studies show that these changes in stress may affect both the seismic and aseismic slip behavior of nearby faults. For instance, they can trigger or delay earthquakes, produce afterslip, influence secular creep rates and trigger creep events. Two types of stress changes are often examined by researchers. One is the static stress change associated with the faulting process and the other is the dynamic stress change attributed to the transient deformation from the passage of seismic waves.

[4] Most studies of the impact of stress changes during the occurrence of earthquakes upon the fault slip behavior of nearby faults focused on earthquake triggering. Many investigators used a static Coulomb stress model and examined the geographical pattern of subsequent seismic events relative to the pattern of changes in static Coulomb Failure Stress (CFS) (see references in the studies of Harris [1998], Stein [1999], and King and Cocco [2001]). Almost all of them found a positive correlation between either the number (or rate) of aftershocks or the occurrence of subsequent main shocks, and regions of calculated positive change in CFS. Despite the apparent success of this static stress triggering model in explaining many observed changes in seismicity, some researchers favor a dynamic stress triggering model, citing as evidence that long-range interactions between earthquakes are observed where calculated static stress changes are negligible while dynamic

¹Department of Earth and Environmental Sciences, Columbia University, New York, USA.

²Lamont-Doherty Earth Observatory, Columbia University, Palisades, New York, USA.

stresses are significant [Hill *et al.*, 1993; Anderson *et al.*, 1994; Gomberg and Bodin, 1994; Gomberg, 1996; Gomberg *et al.*, 1997]. Numerical studies show that in the near field static and dynamic stress perturbations coexist and they both can affect the receiver faults [Cotton and Coutant, 1997; Belardinelli *et al.*, 1999].

[5] A number of researchers also examined the effect of stress changes from sudden seismic slip of a fault on the creep behavior of either the same or nearby faults. Marone *et al.* [1991] modeled afterslip as the relaxation of a stress perturbation within the upper velocity-strengthening layer, which arises when slip in an earthquake at depth propagates upward from a velocity-weakening region below. The secular creep rate of certain faults also is influenced by individual earthquakes. Lienkaemper *et al.* [1997] report an 18 mm creep event on the Hayward fault in 1996, which marked the end of a period of severely reduced creep on the southern part of the fault that began after the 1989 Loma Prieta earthquake. They remark that this reduction in creep rate was consistent with the reduced static stress changes on the Hayward fault both spatially and temporally. The 1983 Coalinga earthquake also perturbed the creep rate of the nearby creeping segment of the San Andreas fault near Parkfield. Several investigators concluded that the observed time-dependent change in creep rate can be interpreted as a response to the Coalinga-induced static stress change [Mavko *et al.*, 1985; Simpson *et al.*, 1988].

[6] Besides afterslip and perturbation of creep rate, the occurrence of an earthquake also can produce “triggered aseismic fault slip,” which is a form of fault creep coinciding closely in time with a large nearby event while being distinct spatially from the primary rupture [Sylvester, 1986]. It was first observed after the 1968 Borrego Mountain earthquake [Allen *et al.*, 1972], and subsequently detected after the 1979 Imperial Valley [Sieh, 1982; Fuis, 1982], the 1981 Westmorland [Sharp *et al.*, 1986a], the 1986 North Palm Springs [Sharp *et al.*, 1986b; Williams *et al.*, 1988], the 1987 Elmore Ranch and Superstition Hills [Hudnut and Clark, 1989; McGill *et al.*, 1989; Sharp, 1989], and the 1989 Loma Prieta earthquakes [Galehouse, 1990; McClellan and Hay, 1990] as well as the 1992 Landers event sequence [Bodin *et al.*, 1994].

[7] Following the 1968 Borrego Mountain earthquake, Allen *et al.* [1972] concluded that the dynamic strain associated with shaking was a more likely cause of the aseismic slip on the San Andreas fault, because the static shear strain was in the wrong sense for the observed dextral displacements. This has been cited as a main piece of evidence by several other proponents of dynamic triggering mechanism who disregard the possible contributions from changes in static normal stress. In contrast, Simpson *et al.* [1988] examined the impact on the central creeping section of the San Andreas fault from the nearby 1983 M 6.7 Coalinga and 1986 M 5.5 Tres Pinos events. They concluded that the triggered slip could be driven by static strain changes. Thus, unlike the general agreement that static stress changes are responsible for long-term perturbations in creep rates, no consensus has been reached so far regarding the causative mechanism of “triggered aseismic fault slip.”

[8] Regular stick-slip motion observed in the frictional sliding between rock surfaces in the lab led Brace and

Byerlee [1966] to propose it as the mechanism of crustal earthquakes. Subsequently, a spring-slider system often has been used as a simplified fault model to study its slip behavior [Rice and Ruina, 1983; Gu *et al.*, 1984; Rice and Tse, 1986; Gu and Wong, 1991; Boatwright and Cocco, 1996; Roy and Marone, 1996; Belardinelli, 1997; Gomberg *et al.*, 1997, 1998]. When a rate-dependent and state-dependent friction law derived from laboratory experiments [Dieterich, 1979; Ruina, 1983] is assumed for the frictional force, the interaction between the loading system and the sliding surface results in various types of motion for the slider, which could provide useful physical insight into the frictional behavior of real faults.

[9] Except for the quasi-static analysis of Gu *et al.* [1984], most earlier studies adopted a Dieterich–Ruina type of friction law with a single state variable and concentrated on the dynamic instabilities that are analogous to seismic movements of faults. Ruina [1983], however, showed that a two-state-variable friction law with similar structure to its one-state-variable counterpart could provide a better description of experimental results. Furthermore, the two-state-variable law has extra complexity compared with the one-state-variable one and may be more suitable in describing the frictional behavior of real faults. Linear and finite-amplitude stability analyses of the system revealed that a sharp boundary exists between the unstable and conditionally stable states with a constitutive law employing a single state variable [Rice and Ruina, 1983; Gu *et al.*, 1984]. With a two-state-variable law, however, Gu *et al.* [1984] demonstrated that a transitional region characterized by self-driven oscillatory or episodic slip exists close to the stability boundary. Such episodic behavior near the stability transition has been observed in the laboratory [Scholz *et al.*, 1972]. Its similarity with the aseismic slip behavior of real faults was pointed out by Scholz [1990, 1998].

[10] The spring-slider system was also used to investigate earthquake triggering by dynamic stresses. Gomberg *et al.* [1997] used a massless system and a one-state-variable friction law to examine transient triggering of an earthquake on one fault by an event on a nearby fault. Their modeling results demonstrated that transient loads do lead to clock advances of future earthquakes and that triggered instabilities may occur after the transient has ceased (i.e., triggering may be delayed). Gomberg *et al.* [1998] further used this simple model to compare the triggering effects of both transient and static deformations. They found that a static stress step imposed late in the earthquake cycle causes less clock advance than an equal step applied earlier, whereas a later imposed transient load leads to greater clock advance than the same one imposed earlier.

[11] The main aim of this study is to evaluate the possible triggering role of changes in static stress and transient loading in producing “triggered aseismic fault slip.” We first use observations of such fault slip motions made after 10 earthquakes in California and a static Coulomb stress model to examine the static triggering scenario. Most of the nearby fault segments that slipped were encouraged to move by the imposed changes in static CFS, but there are three discrepancies with this model, which imply that static stress triggering is either not the sole or not the correct mechanism responsible for causing the observed triggered slip. We then model creep events with a spring-slider system employing a

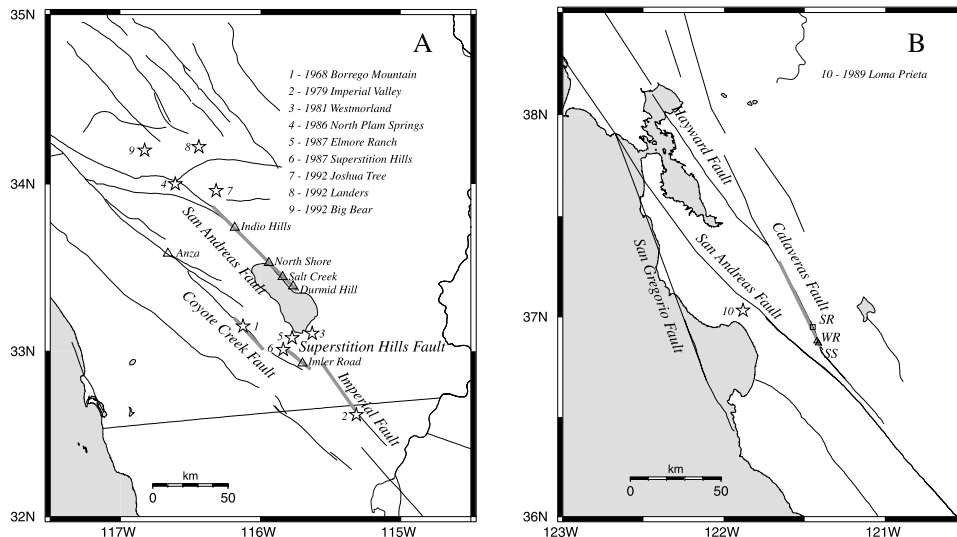


Figure 1. Locations of the 10 earthquakes that triggered creep on nearby faults. (a) Fault map of southern California (32° – 35° N, 114.5° – 117.5° W). Locations of the six creep meter sites that were used to record the triggered slip motion from the 1992 Landers earthquake sequence are denoted by triangles. (b) Region around the epicenter of 1989 Loma Prieta earthquake (36° – 38° N, 120.5° – 123° W) with the locations of the two theodolite sites (WR: Wright Road, SS: Seventh Street) and one creep meter site (SR: Shore Road) near Hollister. Shaded areas indicate the five candidate fault segments in the study region.

two-state-variable rate-dependent and state-dependent friction law and investigate the impact of transient loading on it. Unlike some of the earlier work, we consider the effect of inertia in our numerical analyses. Our modeling shows that certain types of transient loading can cause a large time advance of the anticipated next creep event, which starts shortly after the transient load is applied.

2. Effect of Static Stress Changes

2.1. Data and Methods

[12] As stated previously, “triggered aseismic fault slip” occurred on nearby faults after 10 earthquakes in California (Figure 1). In all of the observed cases, this phenomenon was spatially confined to fault segments that were known to exhibit creep behavior in the absence of nearby shocks. The quality of observational evidence varies from case to case, ranging from geological (visual) observations of surface cracks along the fault surface within several hours of the main shock to a few instrumental recordings that showed that the initiation of creep was confined to the first 1 min after the main shock (Table 1). The depths of the triggered slip events are either poorly resolved or unknown, but are generally assumed to be comparable to the depth of creep on the faults, which is controlled mainly by the local thickness of poorly consolidated sediments. Some evidence exists that the depth of triggered slip events is quite shallow. For example, *Williams et al.* [1988] used an elastic dislocation model to estimate a maximum depth of 120 m for creep events on the San Andreas fault that were triggered by the 1986 North Palm Springs earthquake.

[13] Because the “triggered aseismic fault slip” was confined spatially only to fault segments that were known to have exhibited creep at other times and those fault segments did not experience aseismic fault slip after each

nearby significant event, we call them candidate fault segments. Thus, we look into the possible triggering role of static stress changes by resolving those stress changes associated with each main shock onto candidate fault segments and then examine the signs of static stress changes with respect to whether the triggered slip took place or not on the fault. These candidate fault segments include a portion of the San Andreas fault extending 50 km (80 km in the case of the 1986 North Palm Springs earthquake) from its southern end, the entire Superstition Hills fault with a length of 22.8 km, the whole 30-km-long Coyote Creek fault and the northern 35.2 km of the Imperial fault in southern California. We also include a 50-km-long section of the southern Calaveras fault extending northward from Hollister in central California.

[14] We consider not only the changes in static shear stress, but also the changes in normal stress ($\Delta\sigma$) and CFS (ΔCFS) on the candidate fault segments. These changes are defined as (modified from *Scholz* [1990])

$$\Delta CFS = \Delta\tau + \mu\Delta\sigma$$

where $\Delta\tau$ is the change in shear stress resolved in the direction of slip on the observing fault plane and μ is the effective coefficient of friction. Both $\Delta\tau$ and $\Delta\sigma$ can be calculated directly from elastic theory [*Steketee*, 1958; *Okada*, 1992] after the geometry and slip distribution of an earthquake rupture are defined.

[15] The shear stress is taken to be positive for the direction of slip on the fault and the normal stress is positive for extension. Positive ΔCFS means that a fault is encouraged to move, while a negative value implies that a fault is discouraged from slipping. All of the calculations are performed for a uniform elastic half-space with the program DIS3D [*Erickson*, 1986]. Because the “triggered aseismic

Table 1. Observational Evidence for the Phenomenon of “Triggered Aseismic Fault Slip” on Neighboring Faults After 10 Earthquakes in California^a

Year	Candidate Faults	Slipped?	Geological Observation?	Time Information for the Geological Observation	Length of Slipped Segment (km)	Instrument Recording?	Range of Slip Distance (mm)	
1968	SAF	Yes	Yes	4 days later	30	Yes	10–13	
	SHF	Yes	Yes		23		15–25	
	IF	Yes	Yes		22		8–20	
1979	CCF	No	No	N/A	N/A	No	N/A	
	SAF	Yes	Yes	7 hours to 4.5 days later	39		2–4	
	SHF	Yes	Yes		4 days later		22.5	8–20
1981	CCF	No	No	N/A	N/A	No	N/A	
	SAF	No	No	N/A	N/A		N/A	
	SHF	Yes	Yes	2 days later	15.7		2–14	
1986	IF	Yes	Yes	Same day	16.8	No	2–8	
	CCF	No	No	N/A	N/A		N/A	
	SAF	Yes	Yes	6 days later	17		1.4–9	
1987	SHF	No	No	N/A	N/A	Yes	N/A	
	CCF	Yes	Yes	4 days later	3.9		2–15	
	SAF	Yes	No	N/A	N/A		1–2	
1989	IF	Yes	Yes	4.5 hour after the second shock	19.6	Yes	2–15	
	CF	Yes	Yes		68 and 92 hours later		17	12–14
	SJF	No	No		N/A		N/A	N/A
1992	SAF	Yes	No			Yes	0.2–10	
	SHF	Yes	No				0.2–8.2	

^aAbbreviation for Faults: CCF, Coyote Creek; CF, Calaveras; IF, Imperial; SAF, San Andreas; SJF, San Jacinto; and SHF, Superstition Hills.

fault slip” is generally assumed to have a shallow origin, the calculations are targeted for a depth of 0.5 km. The effective coefficient of friction is taken to be 0.6, and the shear modulus and Poisson’s ratio are fixed at 33 GPa and 0.25, respectively. Table 2 shows the faulting parameters used for the 10 main shocks.

2.2. Results of Stress Calculations

2.2.1. M6.8 Borrego Mountain Earthquake of 9 April 1968

[16] Static changes in shear stress, normal stress and CFS are calculated for the three nearby candidate faults: the southern 50 km of the San Andreas fault, the entire Superstition Hills fault and the northern segment of the Imperial fault (Figure 2). We can see that the entire Superstition Hills fault, which experienced triggered slip, was encouraged to move by the main shock in the sense that the calculated values of Δ CFS are positive (Figure 2b). Although the changes in static shear stress are left-lateral on the three

northwestern sections of the San Andreas fault segment that slipped, the changes in static CFS which takes into account changes in static normal stress are in the correct sense for the observed right-lateral slip (Figure 2a). In contrast, the changes in both static shear stress and CFS are in the wrong sense for the northern 8–10 km of the total 22-km-long Imperial fault segment that slipped aseismically (Figure 2c). This may result from the poorly resolved coseismic faulting model used in the calculation. Several authors studied the waveforms of the 1968 earthquake [Hamilton, 1972; Burdick and Mellman, 1976; Ebel and Helmberger, 1982; Kikuchi and Kanamori, 1985; Petersen et al., 1991]. All of them agreed on the high moment release over the first 6 s but differed about whether seismic moment was released in later subevents. We found that the issue of additional subevents does not affect much the results of our stress calculation because they were reported to be thrust-type events. Since the main rupture extended unilaterally south-eastward, however, if we put more moment release (slip) in

Table 2. Faulting Parameters of the 10 Main Shocks Used for Calculations of Static Stress Changes^a

Event	Segment Number	Length (km)	Depth to Segment Top (km)	Depth to Segment Bottom (km)	Strike (°)	Dip (°)	Segment Center		SS (m)	DS (m)
							Lon (°W)	Lat (°N)		
1968 Borrego Mountain	1	30	0	12.3	311	80 NE	116.10	33.11	1.0	0.0
1979 Imperial Valley	1	35	4.0	13.0	143	90	115.44	32.77	0.59	0
	2	10	0	8.0	180	90	115.48	32.86	0.10	0
1981 Westmorland	1	10	0	5.0	54	90	115.63	33.11	−0.35	0
1986 North Palm Springs	1	22	4	15	287	46 NE	116.63	33.91	0.14	−0.07
1987 Elmore Ranch	1	20	0	12	37	90	115.78	33.08	−0.30	0
1987 Superstition Hills	1	22.7	0	12	126	90	115.74	32.95	1.1	0
1989 Loma Prieta	1	37	5	17.5	136	70 SW	121.91	37.06	1.66	−1.19
1992 Joshua Tree	1	10	0	15	171	90	116.32	34.00	0.5	0
1992 Landers	1	21.2	0	15	135	90	116.66	34.64	1.8	0
	2	23.9	0	15	152	90	116.52	34.48	2.7	0
	3	21.4	0	15	175	90	116.44	34.28	1.8	0
1992 Big Bear	1	20	0	15	48	90	116.77	34.21	−0.8	0

^aSS: Strike-slip component, positive for right-lateral motion; DS: Dip-slip component, positive for normal faulting.

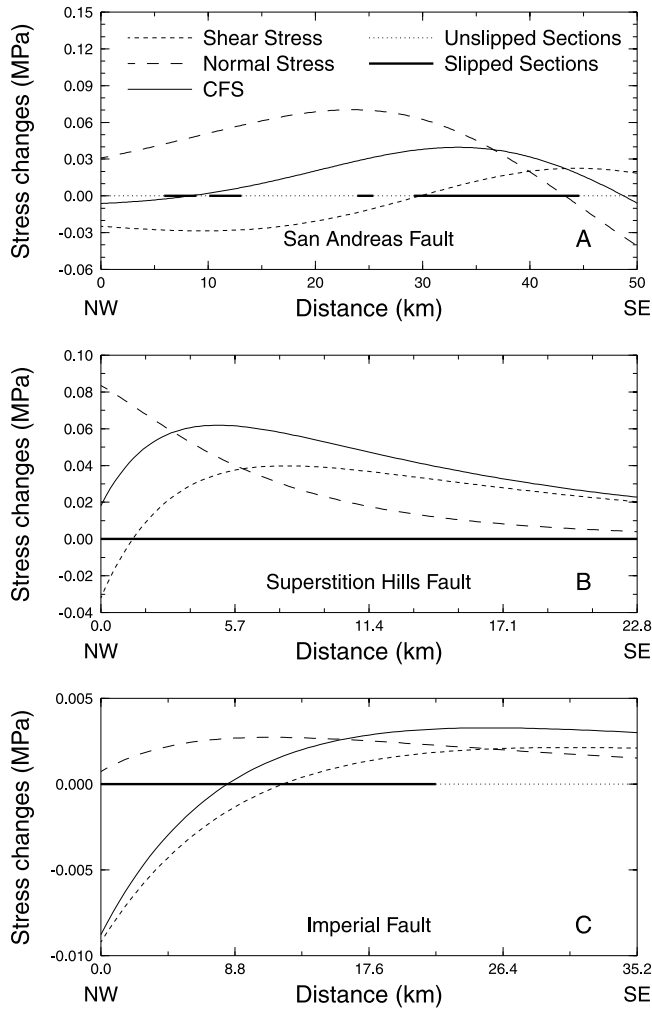


Figure 2. Computed static stress changes from 1968 Borrego Mountain earthquake resolved onto three fault segments: the southern 50 km of the San Andreas fault (a), the entire Superstition Hills fault (b), and the northern 35.2 km of the Imperial fault (c). Distance along each candidate fault segment is measured from its northwestern (NW) to its southeastern (SE) end.

the northwestern part of the rupture plane in the calculation, the negative impact on the northern part of the Imperial fault decreases both in magnitude and affected length without changing the character of the effects on the Superstition Hills and San Andreas faults.

2.2.2. M6.4 Imperial Valley Earthquake of 15 October 1979

[17] Archuleta [1984] constructed a rupture model for this earthquake using near-source, strong motion data. Its prominent feature is that little or no coseismic slip occurred above a depth of 4–5 km, which corresponds to the depth of sediments along the fault. We use his faulting model with coseismic slip extending from depths of 4–13 km and make the stress calculations for the entire Coyote Creek fault, the southern 50 km of the San Andreas fault and the entire Superstition Hills fault (Figure 3). We also compare the above results with another faulting model with coseismic slip extending from surface down to 13 km. Although there

are minor differences in values, the pattern of calculated static stress changes along the faults remain the same. Both the slipped San Andreas fault segment and Superstition Hills fault segment experienced positive changes in static CFS (Figures 3b and 3c). Those for the former, however, are very small. The Coyote Creek fault showed no triggered slip although its southern part underwent very small positive changes in CFS (Figure 3a).

2.2.3. M5.6 Westmorland Earthquake of 26 April 1981

[18] The same stress calculations are made for four candidate faults including the Coyote Creek, the San Andreas, the Superstition Hills, and the Imperial faults (Figure 4). The Imperial and Superstition Hills fault sections, which slipped aseismically, both experienced positive changes in static CFS (Figures 4c and 4d). Those for the Imperial fault, however, are very small. The entire Coyote Creek fault, which did not slip, underwent negative changes in static CFS, while the southern San Andreas fault did not slip despite the very small positive changes in CFS along it.

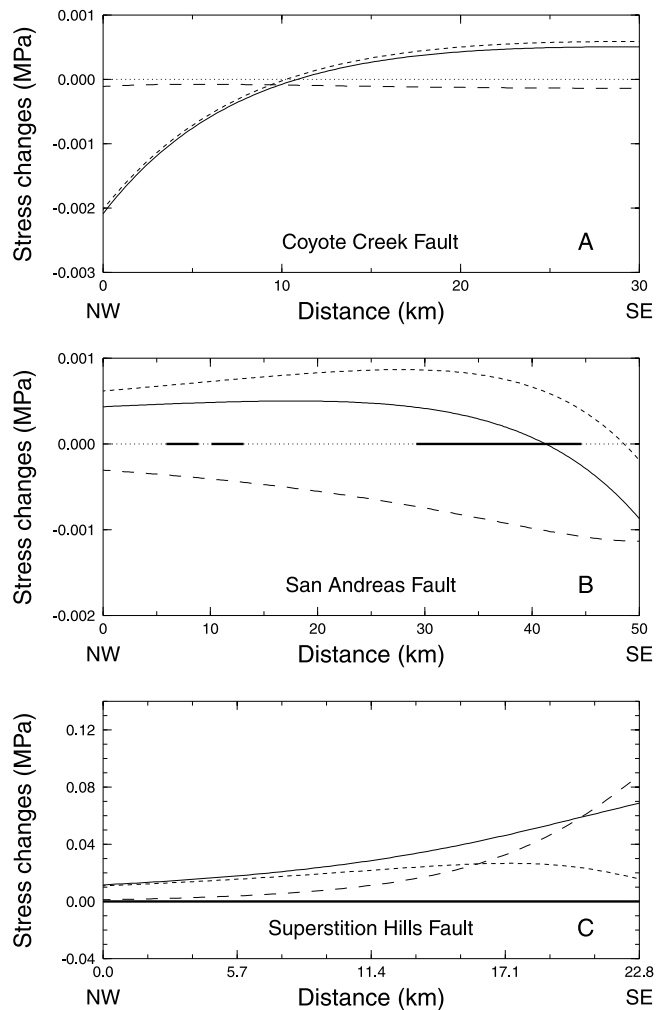


Figure 3. Calculated static stress changes from 1979 Imperial Valley earthquake resolved onto three fault segments: the entire Coyote Creek fault (a), the southern 50 km of the San Andreas fault (b), and the entire Superstition Hills fault (c). Line styles same as Figure 2.

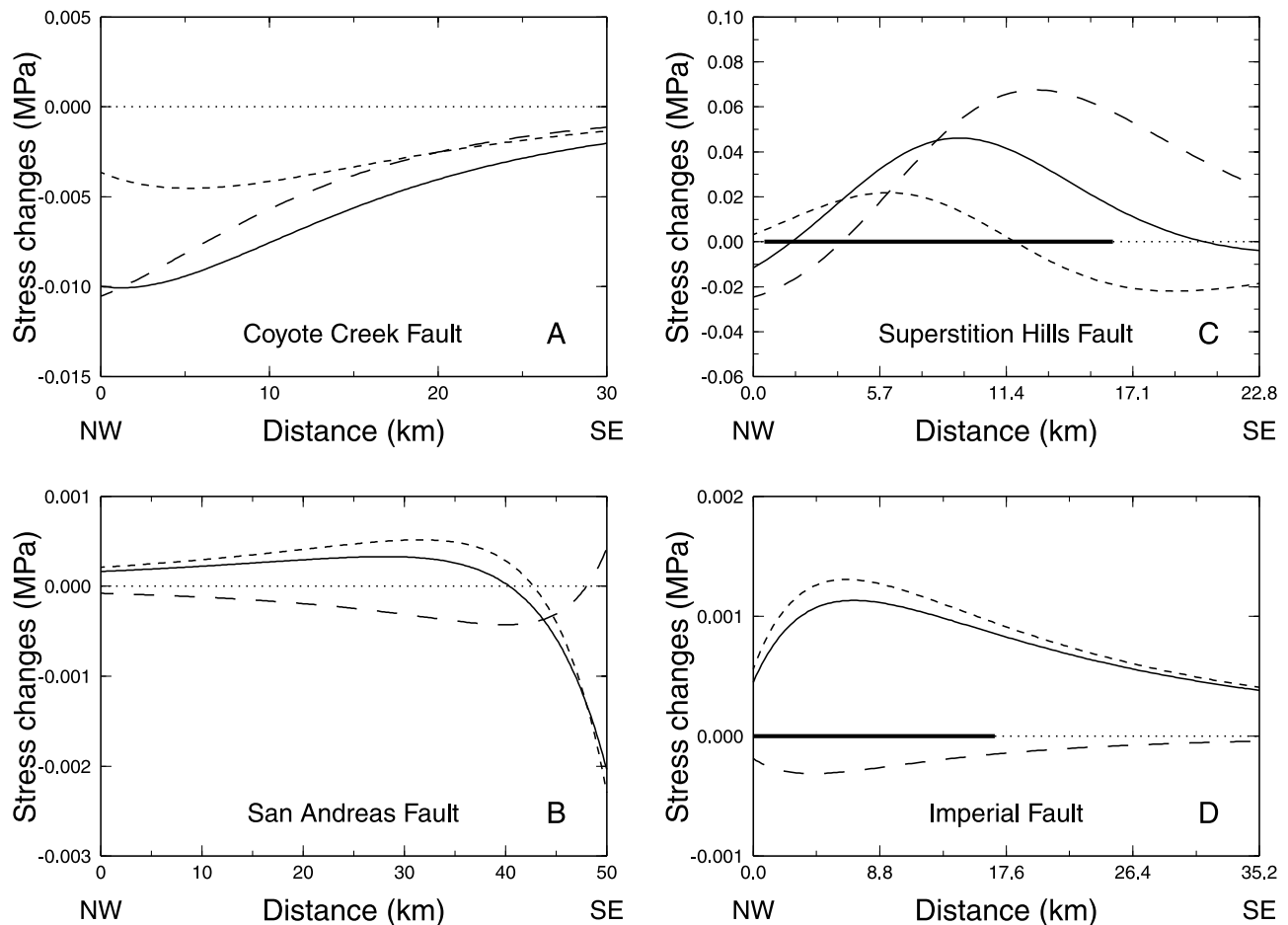


Figure 4. Computed static stress changes from 1981 Westmorland earthquake resolved onto four fault segments: the entire Coyote Creek fault (a), the southern 50 km of the San Andreas fault (b), the entire Superstition Hills fault (c), and the northern 35.2 km of the Imperial fault. Line styles same as Figure 2.

2.2.4. M5.9 North Palm Springs Earthquake of 8 July 1986

[19] Figure 5 shows the results of stress calculations for the Coyote Creek, a 80-km-long section of the San Andreas and the Superstition Hills faults. The changes in static shear stress and CFS for the three slipped sections of the San Andreas fault are all positive for their right-lateral senses of motion (Figure 5b). In contrast, for the Coyote Creek and Superstition Hills faults, which showed no triggered slip, the values of changes in both shear stress and CFS are negative and very small for right-lateral motion (Figures 5a and 5c). Almost no static stress changes are calculated for the Imperial fault, which is farther to the south and experienced no triggered aseismic slip.

2.2.5. M6.2 Elmore Ranch and M6.6 Superstition Hills Events of 24 November 1987

[20] After the two 1987 earthquakes occurred within a 11-hour time interval, *Hudnut and Clark* [1989] found new surface ruptures along the central part of the Coyote Creek fault that ruptured in 1968. *Sharp* [1989] also mapped triggered right-lateral displacements on the surface of Imperial fault. Although the two events failed to produce mappable surface rupture on the San Andreas fault, *McGill et al.* [1989] showed that several millimeters of slip were

recorded by a creep meter at Salt Creek on the San Andreas fault.

[21] Similar static stress calculations are made for the entire Coyote Creek fault, the Imperial, and the San Andreas fault segments. Contributions from the Elmore Ranch event alone and the two main shocks combined are evaluated (Figure 6). Although the static stress changes from the first earthquake discouraged movement along the two Coyote Creek fault segments that slipped aseismically (Figure 6a), the contribution from the second event overcame those negative effects and fostered the right-lateral slippage (Figure 6d). The effect of the Elmore Ranch shock favors right-lateral motion for the entire Imperial fault segment considered (Figure 6b), but the contribution from the Superstition Hills event discouraged the northernmost 6-km-long slipped segment from moving (Figure 6e). Although the net effect from the two events discouraged slip on the northernmost segment, it is possible that the triggered slip on that section occurred during the 11-hour delay between the two events. Unfortunately, there were no instrumental recordings along this segment of the fault to provide information on timing. To the southeast of this fault patch, two alignment arrays and three creep meters were deployed. Except for the most remote creep meter at Turtle Ranch, the other four instru-

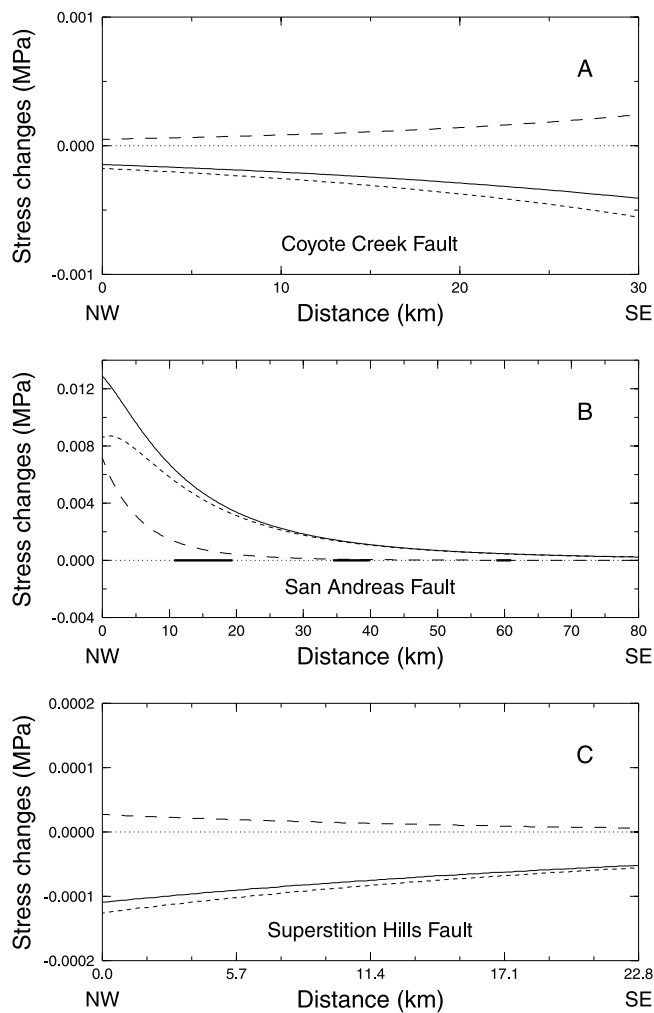


Figure 5. Computed static stress changes from 1986 North Palm Spring earthquake resolved onto three fault segments: the entire Coyote Creek fault (a), the southern 80 km of the San Andreas fault (b), and the entire Superstition Hills fault (c). Line styles same as Figure 2.

ments recorded triggered slip and their site locations experienced positive changes in CFS.

[22] Figures 6c and 6f show the static stress changes resolved on the San Andreas fault segment. We can see that in both cases, the changes in static shear stress and CFS are negative for dextral motion. According to the static stress triggering hypothesis, one would not expect to observe triggered slip on the San Andreas fault. However, the Salt Creek creep meter on the fault recorded dextral slip of 1.3 and 1.7 mm within 3 min of each shock.

2.2.6. M7.1 Loma Prieta Earthquake of 17 October 1989

[23] *Galehouse* [1990] found that the Loma Prieta event apparently triggered up to 12–14 mm of dextral slip on the southern Calaveras fault at two of their theodolite sites (Wright Road and Seventh Street) in the Hollister area. Additional evidence comes from the field observations made by *McClellan and Hay* [1990] who found fresh en echelon cracks and offset features that indicated at least 5 mm of movement along 17 km of the Calaveras fault

northwest of the City of Hollister. The USGS creep meter at Shore Road (8.5 km northwest from Wright Road theodolite) also recorded right-lateral slip of about 5.0 mm. We use a simple one-patch slip model [*Lisowski et al.*, 1990] for the Loma Prieta event and calculate the static stress changes imposed on the southern Calaveras fault segment extending 50 km northwestward from Hollister (Figure 7). We can see that both the changes in shear stress and CFS are negative for the 17-km section of the fault that showed triggered slip. *Simpson and Reasenber* [1994] made a comprehensive study of the static stress changes induced by the Loma Prieta earthquake. They considered three different slip distribution models for the main events including the one we adopt. Despite differences among the various models, the calculated results for all of them show that the changes in static CFS would discourage the 17-km-long fault patch from slipping in a right-lateral sense.

2.2.7. M6.1 Joshua Tree, M7.3 Landers, and M6.2 Big Bear Earthquake Sequence in 1992

[24] *Bodin et al.* [1994] examined data from six functioning creep meters across faults in southern California (Anza station on the San Jacinto fault; Imler Road station on the Superstition Hills fault; Indio Hills, North Shore, Salt Creek and Durmid Hill stations along the San Andreas fault) (Figure 1a). Except for the Anza creep meter on the San Jacinto fault, the other five recorded triggered slip shortly after one or all of the three events in the Landers sequence. Figure 8 shows the static stress changes associated with each of the three shocks at the sites of the six creep meters. For the Anza creep meter on the San Jacinto fault, which did not record triggered slip, the imposed changes in both shear stress and CFS from all three events in the Landers sequence are negative for dextral motion. That part of the San Jacinto fault, however, was not observed to exhibit creep previously [*Louie et al.*, 1985; *Bodin et al.*, 1994], so the Anza creep meter may not record any aseismic motion no matter what kind of stress changes are imposed on that segment. For the other five creep meters, the applied static stress changes from three events all fostered slippage of the fault segments where the creep meters are located, although not a single one of them recorded triggered slip after all three shocks in the sequence.

2.3. Do Static Stress Changes Trigger Aseismic Slip?

[25] Figure 9 shows the relationship between the amount of triggered slip and average changes in static CFS on a fault segment. Most of the fault segments that experienced triggered aseismic motion received positive changes in static CFS resolved in their specific slip directions. There is, however, no simple dependence of the size of positive Δ CFS and the amount of triggered slip from the causative earthquake. Some of those positive values are very small. Seven out of 18 (39%) slipped fault patches received Δ CFS with values smaller than the diurnal change in tidal stress, 0.003 MPa [*Melchior*, 1983], and 61% of them experienced values of Δ CFS less than those of the smallest stress level, 0.01 MPa, that has been reported for the triggering of nearby earthquakes [*Anderson and Johnson*, 1999]. Some researchers, however, argued that static stress changes smaller than 0.01 MPa also have a noticeable triggering effect for earthquakes [*Nalbant et al.*, 1998; *Ziv and Rubin*, 2000]. Creep events are generally believed to have shallow

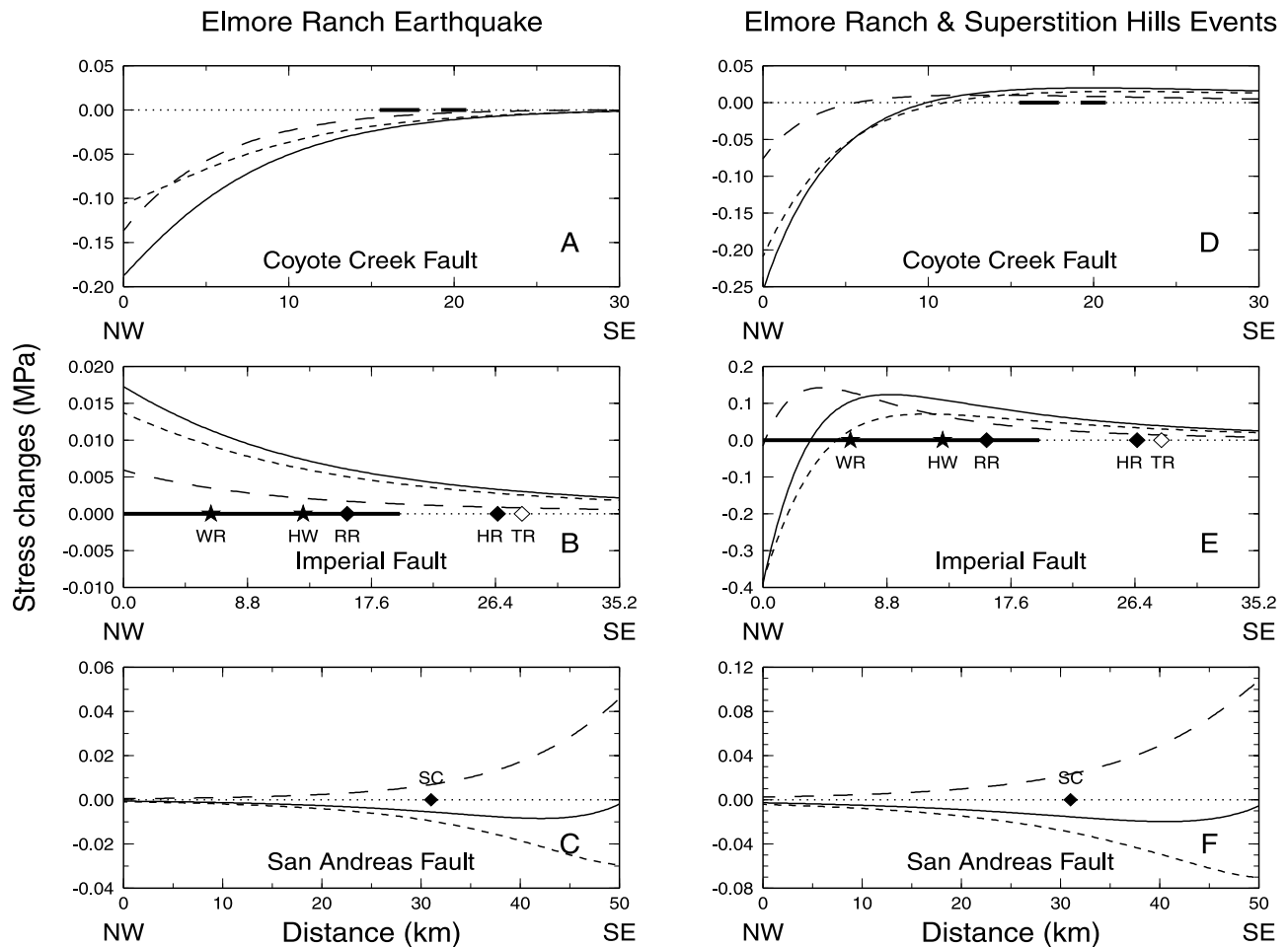


Figure 6. Computed static stress changes from 1987 Elmore Ranch earthquake alone and those combined with the 1987 Superstition Hills shock resolved onto three fault segments: the entire Coyote Creek fault (a and d), the northern 35.2 km of the Imperial fault (b and e), and the southern 50 km of the San Andreas fault (c and f). Instruments that recorded triggered fault slip are denoted with filled symbols and those that did not are denoted with unfilled symbols. (WR: Worthington Road alignment array; HW: Highway 80 alignment array; RR: Ross Road creep meter; HR: Heber Road creep meter; TR: Tuttle Ranch creep meter and SC: Salt Creek creep meter.) Line styles same as Figure 2.

origins where the stress levels are much lower than those at depths of several kilometers at which earthquakes occur and are triggered. Whether some of those very small positive ΔCFS the faults received could trigger their observed slippage in creep events is questionable.

[26] Three discrepancies also exist for the static triggering hypothesis. The southern San Andreas and the southern Calaveras fault segments have negative calculated changes in static CFS associated with both events in the 1987 Superstition Hills earthquake sequence and the 1989 Loma Prieta event respectively. According to the static stress triggering model, we would not expect to observe triggered fault slip on those fault patches. Nonetheless, the Salt Creek creep meter deployed on the southern San Andreas fault recorded dextral slip of 1.3 mm (-0.005 MPa) and 1.7 mm (-0.01 MPa) right after each event in the 1987 sequence. The shore road creep meter on the southern Calaveras fault recorded slip of 5 mm right after the 1989 shock, although the mean ΔCFS that patch of the fault received is about -0.05 MPa.

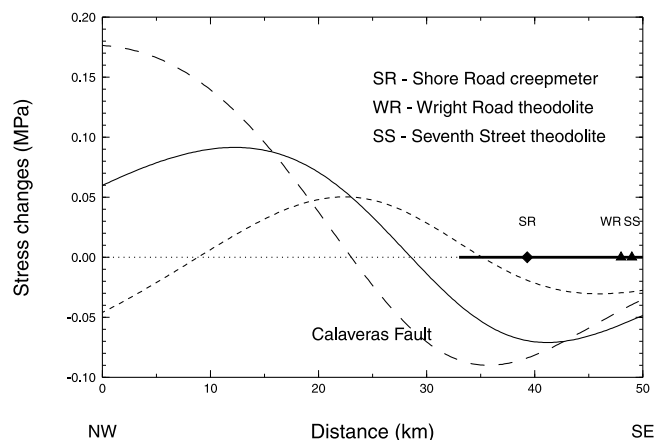


Figure 7. Calculated static stress changes from 1989 Loma Prieta earthquake resolved onto the southern Calaveras fault segment (50 km long extending northwest from Hollister). Line styles same as Figure 2.

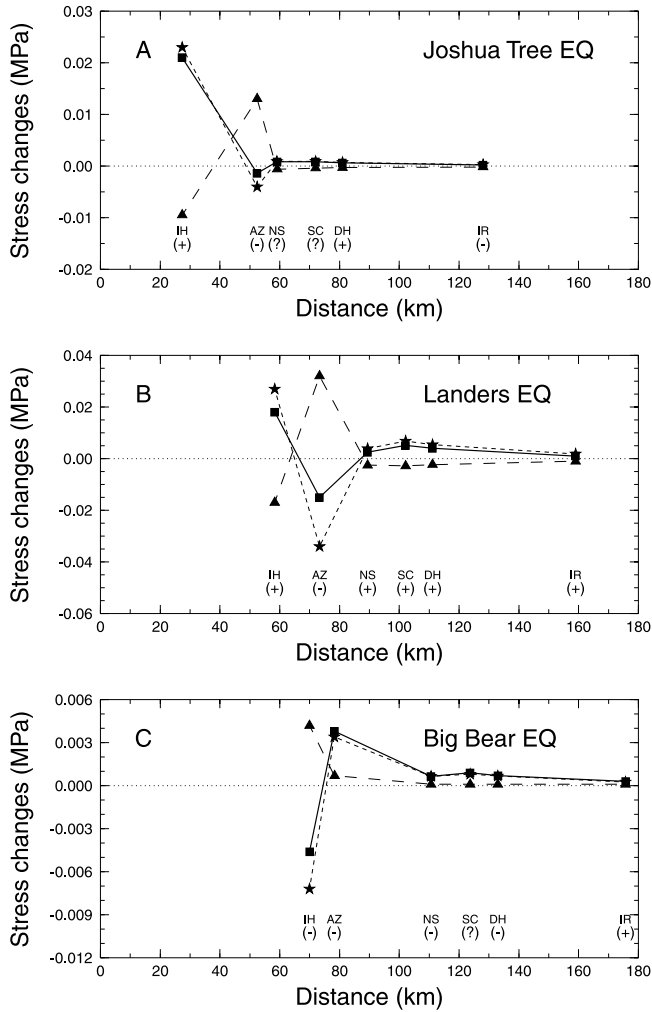


Figure 8. Static stress changes from the 1992 Joshua Tree, Landers, and Big Bear earthquakes calculated for the locations of six creep meters (AZ: Anza; IH: Indio Hills; NS: North Shore; SC: Salt Creek; DH: Durmid Hill, and IR: Imler Road). Calculated changes in shear stress are denoted by short dashed lines and stars. Those in normal stress changes are represented by long dashed line with square symbols, and changes in CFS are designated by solid line with triangular symbols. Plus sign (+) means triggered creep event was detected at a certain creep meter and minus sign (-) indicates no creep event was detected, while question mark (?) represents uncertain signal.

[27] Another hypothesis is that triggered aseismic slip is promoted by static increases in normal stress, i.e., extensional stress or “unclamping” of the fault. We can see in Figure 2a that positive normal stress changes, which are extensional, are associated with the patches of the San Andreas fault that slipped in 1968. When we examine this “unclamping effect” for the other cases, however, we find that several slipped fault segments experienced compressional stress changes from nearby earthquakes. Hence, we think that the “unclamping” effect alone is not responsible for triggering the aseismic fault slip. In our stress calculations, we use a μ equal to 0.6, but we do not know whether this value is applicable to materials in fault zones at very

shallow depth. Since the “unclamping” effect is not prominent, changing the friction coefficient to a smaller value does not affect our main results very much.

[28] A common practice in static Coulomb stress analysis is using an effective coefficient of friction μ to account for the contribution from pore pressure changes. *Beeler et al.* [2000] discourage this usage and argue that other pore pressure models, such as homogeneous isotropic poroelastic response, may be more appropriate for describing earthquake faulting and aftershocks under some circumstances. *Cocco and Rice* [2002] further examine the effects of pore pressure and poroelasticity in static Coulomb stress analysis. They show that pore pressure changes are determined by fault-normal stress changes when the shear modulus within the fault zone is significantly smaller than that in the surroundings but by mean stress changes when the elastic mismatch is small. We find that while adopting a different poroelastic model can affect the amount of CFS change a candidate fault experienced, it does not change the fact that three slipped fault segments received negative changes in CFS when calculated as in by *Beeler et al.* [2000, Figure 5] shows that the southern 17 km of the Calaveras fault, which experienced triggered aseismic slip, received negative CFS changes from the 1989 Loma Prieta earthquake under two different poroelastic models). Combined with the observation that some of the positive Δ CFS the candidate fault segments underwent are very small, they imply that the static stress triggering either is not or is not the sole mechanism causing the observed triggered slip.

3. Effects of Transient Loading

[29] As shown above, the static stress triggering mechanism cannot explain all observed “triggered aseismic fault slip” from nearby earthquakes in the sense that some of the slipped fault segments received negative changes in static CFS. Thus, we proceed to evaluate the triggering role of transient (dynamic) loading but to deal with it from a different perspective. First we use a spring-slider system as a very simplified fault model and simulate repeating creep events by assuming a two-state-variable rate-dependent and state-dependent frictional law. We then introduce transient loads into the system and examine its response. Specifically we are interested in knowing whether the timing of the anticipated creep event can be “clock advanced” (or triggered) by the transient loading and, if so, under what circumstances.

3.1. Governing Equations

[30] Figure 10 shows the spring-slider system that we use as a fault model to study its slip behavior. The slider with mass m is loaded by a spring of stiffness K that is connected to a moving loading point and is resisted by a frictional force τ . Taking into account of the effect of inertia, the equation of motion for the slider is

$$mg = m dV/dt = K(\delta_{lp} - \delta) - \tau$$

Where t is the time; δ , V , and g are respectively the slider displacement, velocity, and acceleration; δ_{lp} is the load point displacement. The frictional force τ is assumed to obey a

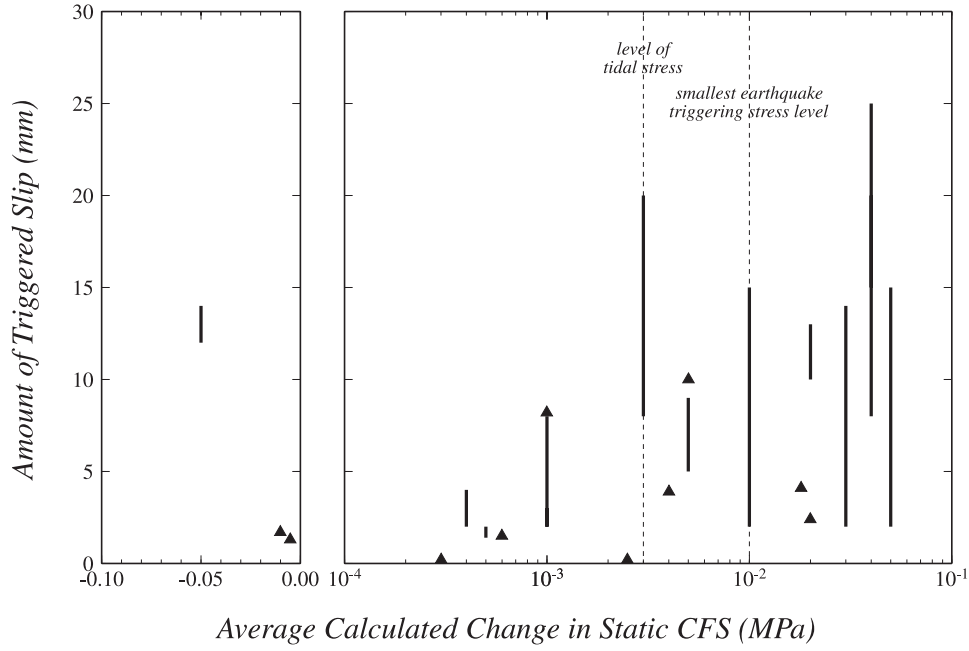


Figure 9. Relationship between the amount of triggered slip and the average calculated changes in static CFS on a fault segment (thick vertical line) or at the site of a creep meter (triangle). Note that positive CFS are plotted with a logarithmic scale at right while a linear scale is used for the negative static stress changes at left.

two-state-variable law of *Ruina* [1983] under constant normal stress σ :

$$\begin{aligned} \tau &= \tau_* + \theta_1 + \theta_2 + A \ln(V/V_*) \\ d\theta_1/dt &= -(V/L_1)[\theta_1 + B_1 \ln(V/V_*)] \\ d\theta_2/dt &= -(V/L_2)[\theta_2 + B_2 \ln(V/V_*)] \end{aligned}$$

Where τ_* is the reference friction level at an arbitrary slip velocity V_* ; θ_1 and θ_2 are the two state variables with critical slip distances of L_1 and L_2 ; A , B_1 and B_2 are coefficients which characterize respectively the instantaneous response and evolution of frictional force when the slider undergoes a sudden velocity perturbation.

[31] Following the study of *Gu et al.* [1984], we can rewrite the above equations using the following dimensionless quantities: mass $M \equiv 2mV_*^2/A(L_1 + L_2)$, stiffness $k \equiv K(L_1 + L_2)/2A$, time $T \equiv 2V_*t/(L_1 + L_2)$, displacement $X_s \equiv 2\delta/(L_1 + L_2)$, velocity $U \equiv V/V_*$, acceleration $G \equiv g(L_1 + L_2)/2V_*^2$, frictional stress $f \equiv (\tau - \tau_*)/A$, state variable one $\xi_1 \equiv \theta_1/A$, state variable two $\xi_2 \equiv \theta_2/A$, constants $\beta_1 \equiv B_1/A$, $\beta_2 \equiv B_2/A$ and $\rho \equiv L_1/L_2$. We then get the following ODE equations:

$$dG/dT = [k(U_{lp} - U) - df/dT]/M \quad (1)$$

$$df/dT = d\xi_1/dT + d\xi_2/dT + G/U \quad (2)$$

$$d\xi_1/dT = -U \left(1 + \frac{1}{\rho} \right) [\xi_1 + \beta_1 \ln(U)]/2 \quad (3)$$

$$d\xi_2/dT = -U(1 + \rho)[\xi_2 + \beta_2 \ln(U)]/2 \quad (4)$$

$$dX_s/dT = U \quad (5)$$

[32] Also we have an equation for the evolution of the load point displacement X_{lp} and velocity U_{lp} :

$$dX_{lp}/dT \equiv U_{lp} = U_b + U_r \quad (6)$$

where U_b is the background loading velocity and U_r is the change to the load point velocity from the passage of the transient waves.

[33] *Rice and Tse* [1986] showed that two timescales are involved in the temporal evolution of the slider system when the effect of inertia is considered. One is the inertia timescale set by the natural oscillation period of the corresponding frictionless slider system

$$\frac{T_o}{2\pi} \equiv \sqrt{\frac{m}{K}} = \sqrt{\frac{M}{k} \frac{L_1 + L_2}{2V_*}}$$

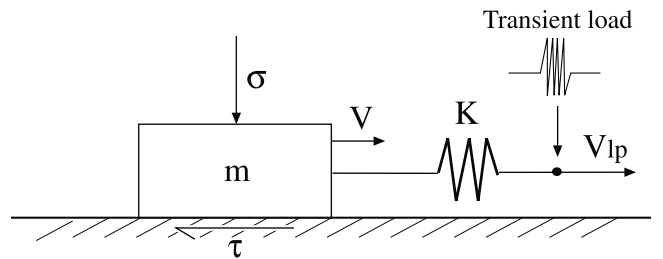


Figure 10. A simple spring-slider system. A slider with mass m under constant normal stress σ is pulled by a spring that is connected to a loading point. Spring constant is K and load point is moving with a velocity V_{lp} , which is kept as a constant until a transient load is applied.

The other is a state relaxation timescale associated with the evolution of frictional stress toward a steady state over a characteristic slip distance

$$T_s \equiv \frac{L_1 + L_2}{2V} = \frac{L_1 + L_2}{2UV_*}.$$

The ratio between the two timescales

$$\lambda \equiv \frac{T_o}{2\pi} / T_s = U \sqrt{\frac{M}{k}}$$

controls the numerical calculation of the temporal evolution of the slider system. When the system is in a relaxation regime ($\lambda \ll 1$), the inertia of the slider can be neglected and a quasi-static analysis can describe fully the temporal evolution of the slider system. In this regime, (1) and (2) can be simplified to

$$df/dT = k(U_{lp} - U) \quad (7)$$

$$G = 0 \quad (8)$$

3.2. Numerical Calculation Procedures

[34] Since the dynamics of the slider system is governed by a set of ODE equations, either (3)–(8) in the relaxation regime ($\lambda \ll 1$) or (1)–(6) otherwise, we solve them using a fifth-order Cash-Karp Runge-Kutta method with adaptive step size control [Press *et al.*, 1992]. Starting with the initial conditions, we compute the value of λ at the end of each time step and compare it with a small value λ_s . If $\lambda \leq \lambda_s$, we carry out the calculations in the next time step using quasi-static equations (3)–(8); otherwise we use (1)–(6) which take into account of the effect of inertia. Similar to what Rice and Tse [1986] used, λ_s is set to 5×10^{-4} .

3.3. Parameters and Initial Conditions

[35] A number of parameters must be specified for the system: M , k , β_1 , β_2 , ρ and U_{lp} . Gu and Wong [1991] examined the effects of loading velocity, stiffness, and inertia on the dynamics of a spring-slider system governed by a one-state-variable friction law. Following them we use $M_* = 7.0 \times 10^{-17}$ as a reference value for mass, which corresponds to $T_0 = 5$ s for a stiffness of 10 MPa/m. As shown by Rice and Ruina [1983] and Gu *et al.* [1984], the values of β_1 , β_2 and k determine the stability regimes of the slider system. The system is velocity weakening when $\beta_1 + \beta_2 > 1$ and velocity strengthening when $\beta_1 + \beta_2 < 1$. In the velocity-weakening regime, a critical stiffness k_c exists. The system is conditionally stable when $k > k_c$ and unstable for $k < k_c$. A transition region characterized by self-driven oscillatory motion also exists close to the stability boundary. In their quasi-static analysis of the system, Gu *et al.* [1984] determined the critical stiffness as:

$$k_c^{quasi} = \frac{[(\beta_1 - 1) + \rho^2(\beta_2 - 1) + 2\rho(\beta_1 + \beta_2 - 1)]}{\sqrt{[(\beta_1 - 1) + \rho^2(\beta_2 - 1)]^2 + 4\rho^2(\beta_1 + \beta_2 - 1)}/4\rho}$$

When the effect of inertia is included, we find the critical stiffness is

$$k_c = \frac{k_c^{quasi} \left(1 + \frac{M(1+\rho)^2}{2\rho}\right)}{\frac{M(\beta_1 + \beta_2 - 1)(1+\rho)^2}{4\rho}}.$$

Since $M \ll 1$, the value of k_c is very close to that of k_c^{quasi} . We use a parameter $k_* \equiv k/k_c$ to specify the stiffness k relative to k_c . Ruina [1980, 1983] determined the parameters in the two-state-variable friction law for experiments performed by Dieterich [1981] and Ruina [1980, 1983]. He obtained one set of parameters for a constant normal stress $\sigma = 100$ bars: $\rho = 0.27$ with $L_1 = 20$ μm and $L_2 = 75$ μm , $A/\sigma = 0.015$, $\beta_1 = 0.67$ and $\beta_2 = 0.60$. We use this set of ρ , β_1 and β_2 as reference values in the following analysis.

[36] Following the study of Gu and Wong [1991], we assume that initially the system slides steadily at the reference velocity V_* , and then suddenly the load point velocity is perturbed to a background loading level that remains constant ($U_{lp} = U_b$) throughout the numerical calculation except for the time duration when a transient load is introduced into the system. Thus, the initial conditions are $U = U_{lp} = 1$ for $t \leq 0$ and $U_{lp} = U_b$ for $t > 0$ except for the transient loading time period.

3.4. Background Loading Only ($U_{lp} = U_b$)

[37] When there is only background loading on the system ($U_{lp} = U_b$ for $t > 0$), the slider moves stably at velocity $U = U_b$ if the system is in either the velocity-strengthening ($\beta_1 + \beta_2 < 1$) or the conditionally stable regimes ($\beta_1 + \beta_2 > 1$ and $k > k_c$). Thus, we concentrate on the slider motions in the velocity-weakening regime with $k \leq k_c$.

[38] Figure 11 shows the evolution of the slider system for $k_* = 0.70$, $U_b = 1.2$ and the set of reference values ($\beta_1 = 0.67$, $\beta_2 = 0.60$, $\rho = 0.27$ and $M = 7.0 \times 10^{-17}$). We can observe the cyclic stick-slip movements of the slider, which are thought to be analogous to recurrent earthquakes. In each cycle, immediately after the previous dynamic motion is arrested, the slider velocity (Figure 11d) builds up quasi-statically until the inertia effect dominates ($\lambda = U\sqrt{M/k} \geq \lambda_s$). Subsequently the slider accelerates to a peak velocity U_{max} and undergoes a stress drop Δf , which is defined as the difference between the maximum and minimum friction levels (Figure 11c) attained in the cycle [Gu and Wong, 1991].

[39] We investigate the effect of k_* on U_{max} and Δf and the results are shown in Figure 12. Overall the values of both U_{max} and Δf decrease with increasing k_* , except for two k_* values near 0.76 and 0.85. Detailed examination reveals that the slider displays various types of motions for different subregions of k_* . In subregion A ($0 < k_* < 0.76$), the slider shows pure cyclic dynamic motion similar to what is depicted in Figure 10. Two-cycle motion occurs for subregion B ($0.76 \leq k_* < 0.85$) where the first cycle has a much smaller peak velocity than the second. The slider displays multicycle motions for subregion C ($0.85 \leq k_* \leq 0.90$). Two-cycle motion reoccurs for subregion D ($0.90 < k_* < 0.92$) and pure cyclical motion reappears in subregion E ($0.92 \leq k_* \leq 1.0$). An important feature we observe is that the values of U_{max} are in a very tight range for $k_* \leq 0.90$ and decrease rapidly to very low values when k_* approaches 1.0.

[40] Subregion E is our focus in this study. If we use k_*^c to represent its lower boundary, then $1 - k_*^c$ is the size of

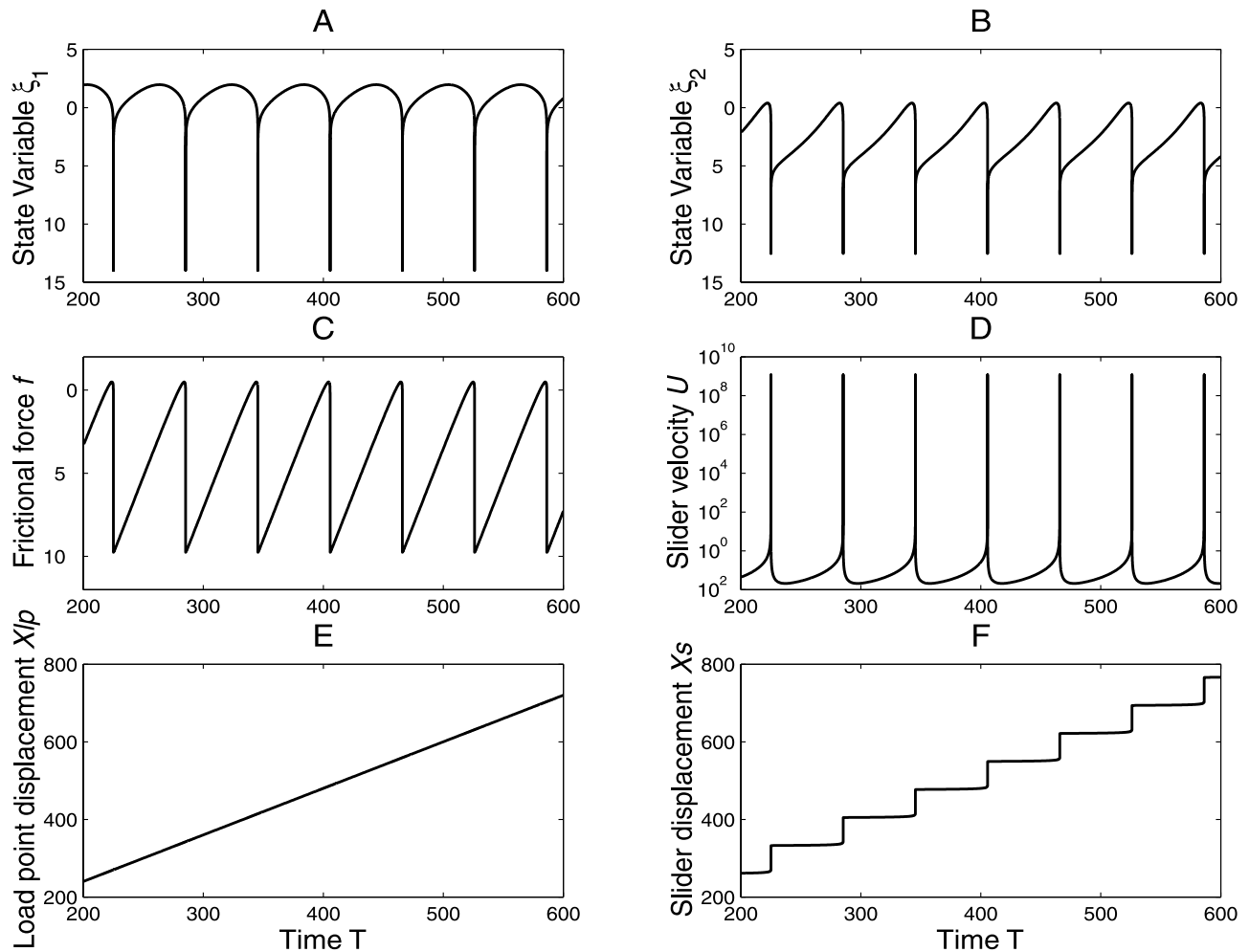


Figure 11. Temporal evolution of the slider system for $k_* = 0.70$ with parameters $\beta_1 = 0.67$, $\beta_2 = 0.60$, $\rho = 0.27$, $M = 7.0 \times 10^{-17}$, and $U_b = 1.2$.

subregion E. Figure 13 shows the change of $1 - k_*^c$ with ρ , the ratio of the two critical slip distances L_1 and L_2 (We do not consider the scenario of $\rho > 1$, since it is equivalent to the case of $\rho' = 1/\rho < 1$ with the values of β_1 and β_2 interchanged). The size of the subregion E reaches a maximum value for $\rho \approx 0.15$ and decreases when ρ approaches either 0 or 1. This pattern is what we expected since the two-state-variable law degenerates into its one-state-variable counterpart when the value of ρ gets very close to either 0 or 1.

3.5. Modeling of Creep Events and Scaling to Actual Faults

[41] Numerous studies were taken to understand the phenomenon of fault creep since its discovery. Many of them were mainly concerned with the temporal shape of a single creep event or its propagation along a fault [Nason and Weertman, 1973; Ida, 1974; Stuart et al., 1985; Wesson, 1988]. Nason and Weertman [1973] analyzed the displacement history of creep events based on models of propagating edge and screw dislocations. They assumed that a creeping fault could be modeled by a slab of time-deformable and nonelastic materials separating two elastic quarter-spaces and argued that fault creep can be interpreted as a

yield point phenomenon. Wesson [1988] further considered viscous and power law creep rheologies for the nonelastic fault zone material and derived a matrix formulation to explain propagating creep events. Bilham and Behr [1992] proposed a two-layer model for aseismic slip on the Superstition Hills fault. They argued that stable sliding occurs from the surface to a transition depth, below which episodic creep events are initiated. That zone was taken to be located above the seismogenic layer.

[42] Scholz [1990, 1998] pointed out the similarity of slider motion close to the stability boundary with aseismic slip behavior of real faults. We also think that the slider movement in subregion E is a reasonable conceptual model for the phenomenon of fault creep events. Figure 14 shows the periodic slider motion for $k_* = 0.96$. In each cycle, the slider slips quasi-statically before reaching a much smaller peak velocity U_{max} than that in Figure 11d. It never enters the inertia-controlled regime. Periodic step increases in slider displacement profile (Figure 14f) mimic the periodic aseismic (creep) events observed on creeping faults.

[43] Field observations of creep events show that they consist of small episodes of slow sliding with typical amplitudes of the order of a few millimeters, characteristic times of the order of hours to days and recurrence times of

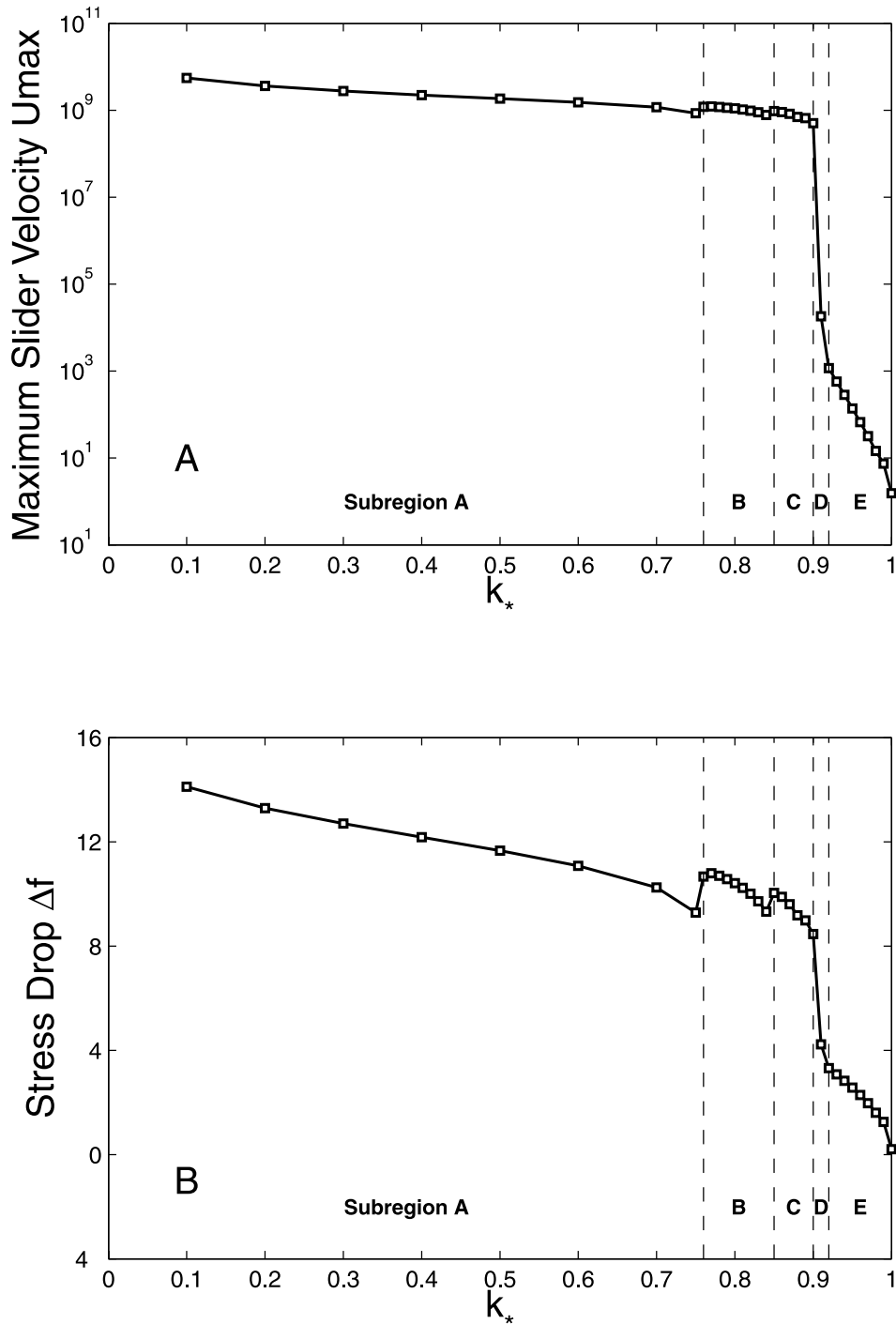


Figure 12. Changes in maximum slider velocity U_{max} (a) and stress drop Δf (b) with k_* for the set of parameters: $\beta_1 = 0.67$, $\beta_2 = 0.60$, $\rho = 0.27$, $M = 7.0 \times 10^{-17}$, and $U_b = 1.2$. The five subregions are separated by the vertical dotted lines.

tens to hundreds of days. Our modeled creep event in Figure 14 has a duration around 0.5, a recurrence time of about 14 and a slip distance around 15. Since our numerical analysis uses nondimensional variables, we can obtain the dimensional time and slip distance using $t = \frac{L_1+L_2}{2V_*} T$ and $\delta = \frac{L_1+L_2}{2} X_*$. If we use 3×10^{-10} m/s for V_* , which corresponds to a $U_b \approx 10$ mm/yr, $L_1 = 20 \mu\text{m}$ and $L_2 =$

$75 \mu\text{m}$ [Ruina, 1980, 1983], we get the duration, recurrence time, and slip distance of our modeled creep events as 1.2 days, 34 days, and 0.7 mm. Thus, our modeled events have reasonable scales of duration, recurrence time and slip distance compared to those of actual fault creep events. Observations showed that the shapes of real creep events recorded at a specific site are usually similar but vary

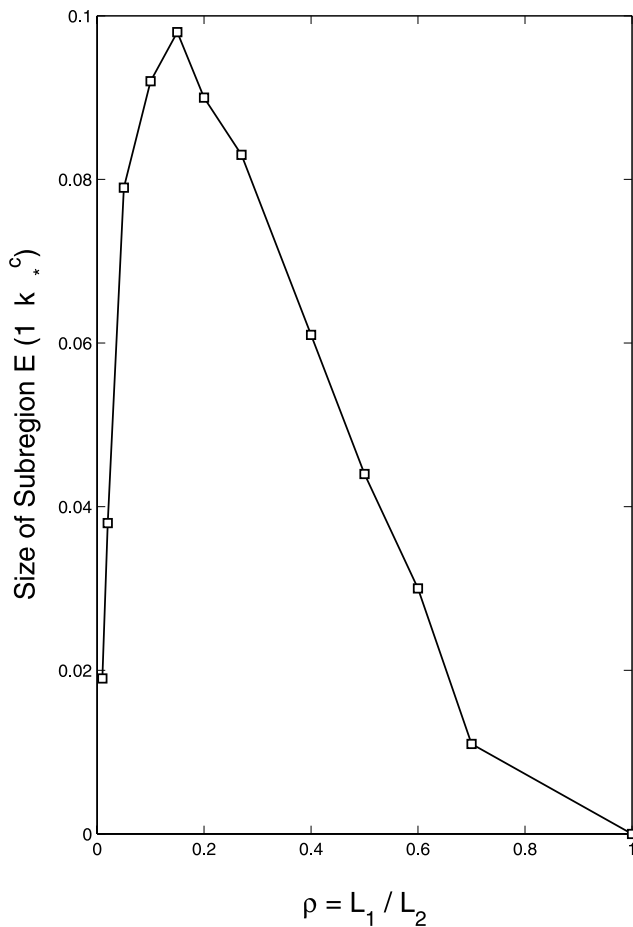


Figure 13. Changes in size of subregion E, $1 - k_c^c$, with ρ , the ratio of two critical slip distances L_1 and L_2 . Other parameters are $\beta_1 = 0.67$, $\beta_2 = 0.60$, $M = 7.0 \times 10^{-17}$, and $U_b = 1.2$.

among sites [Wesson, 1988]. Hence, we do not expect our modeled creep events to display the same time history as real ones, but rather to provide some physical insight into this phenomenon.

3.6. A Modified Model of Frictional Stability for Faults

[44] The introduction of rate-dependent and state-dependent frictional laws has revolutionized studies of crustal faulting. Various earthquake phenomena can be understood in the context of this constitutive law [see review by Scholz, 1998]. Previous studies found that the frictional behavior of real crustal faults depends on material properties of fault zones, which are controlled by temperature, pressure as well as lithology, and thus are depth dependent [Dieterich, 1978; Stesky, 1978; Tse and Rice, 1986; Scholz, 1990].

[45] Figure 15 is a synoptic model of frictional stability for faults as a function of depth, modified from the one in the study of Scholz [1998]. The frictional regime of shallow part of faults under low normal stress is velocity strengthening, which is usually denoted as $a - b > 0$ in terms of the one-state-variable frictional law or equivalently as $\beta_1 + \beta_2 < 1$ under its two-state-variable counterpart. A fault enters the velocity-weakening regime ($a - b < 0$ or $\beta_1 + \beta_2 > 1$) at h_1 , the depth of an “upper stability transition.” As depth

increases, a “lower stability transition” at depth h_6 is reached, and the fault behavior changes again to velocity strengthening and stable sliding.

[46] Below the “upper stability transition,” the value of $\beta_1 + \beta_2 - 1$, or equivalently the critical stiffness k_c , increases from zero as depth increases. Consequently the ratio k_* between stiffness k , which is equal to $K(L_1 + L_2)/2a\sigma$, and k_c decreases from a large number toward 1.0. Thus, the fault enters a conditionally stable regime. With further increase in depth and normal stress σ , the value of k_* drops below 1.0 but lies above k_*^c , the lower boundary of subregion E in Figure 12, for depths from h_2 to h_3 . It is in this particular layer that we think creep events originate. The seismogenic zone where crustal earthquakes occur is located below it. The thickness of this layer, $h_3 - h_2$, depends on the properties of fault zone materials and is likely to vary along strike and among different faults. Thus, stable sliding (or secular creep) occurs in both the shallow velocity-strengthening and the conditionally stable regions; episodic creep events originate in a layer below. This fault creep configuration is similar to the two-layer creep model of *Bilham and Behr* [1992]. They, however, did not base their model on a frictional law as we do. *Belardinelli* [1997] also modeled creep events on a fault in terms of a spring-block system. Instead of using a two-state-variable friction law as we do, she used a one-state-variable law modified from that proposed by *Ruina* [1980]. She, however, focused more on explaining increasing interevent times in creep event sequences using time-dependent fault parameters.

[47] By symmetry, another layer below the seismogenic zone exists from depth h_4 to h_5 , where the frictional behavior is velocity weakening and the value of k_* belongs to subregion E ($k_*^c \leq k_* < 1.0$). We think that similar creep events as those in the shallower layer also originate in this region.

[48] Besides creep events, which typically involve small amounts of slip, larger-scale aseismic fault slip events exist, so-called slow earthquakes. *Linde et al.* [1996] report a slow earthquake sequence on the San Andreas fault with an equivalent magnitude of 4.8. They limited the top of the source area to be 100–300 m from the Earth’s surface but were unable to get a good control on the bottom depth. *Miller et al.* [2002] report eight nearly periodic slow earthquakes from the Cascadia subduction zone with a 14.5-month average recurrence time. Their modeling work suggests the depths of these slow events are below the locked zone, which may fit into the layer h_4 and h_5 in Figure 15. The mechanisms of these slow earthquakes are generally unknown. Our modeling work suggests that they may be just larger versions of creep events and originate under similar conditions.

3.7. Impact of Transient Loading ($U_{lp} = U_b + U_{tr}$)

[49] *Gomberg et al.* [1997] used a massless spring-slider system to investigate transient triggering of an earthquake on one fault by an event on a nearby fault. They modeled the propagating seismic waves from the latter to the former using a sine wave scaled by a Gaussian pulse. We use a sine wave transient, i.e., a sine wave that turns on and then off abruptly, to simulate the passage of the waves radiated by a nearby earthquake. Thus,

$$U_{lp} = U_b + U_{tr} = U_b + A \sin \left[\frac{2\pi(T - T_b^{tr})}{T_b^{tr}} \right] (T_b^{tr} \leq T \leq T_b^{tr} + N \cdot T_b^{tr})$$

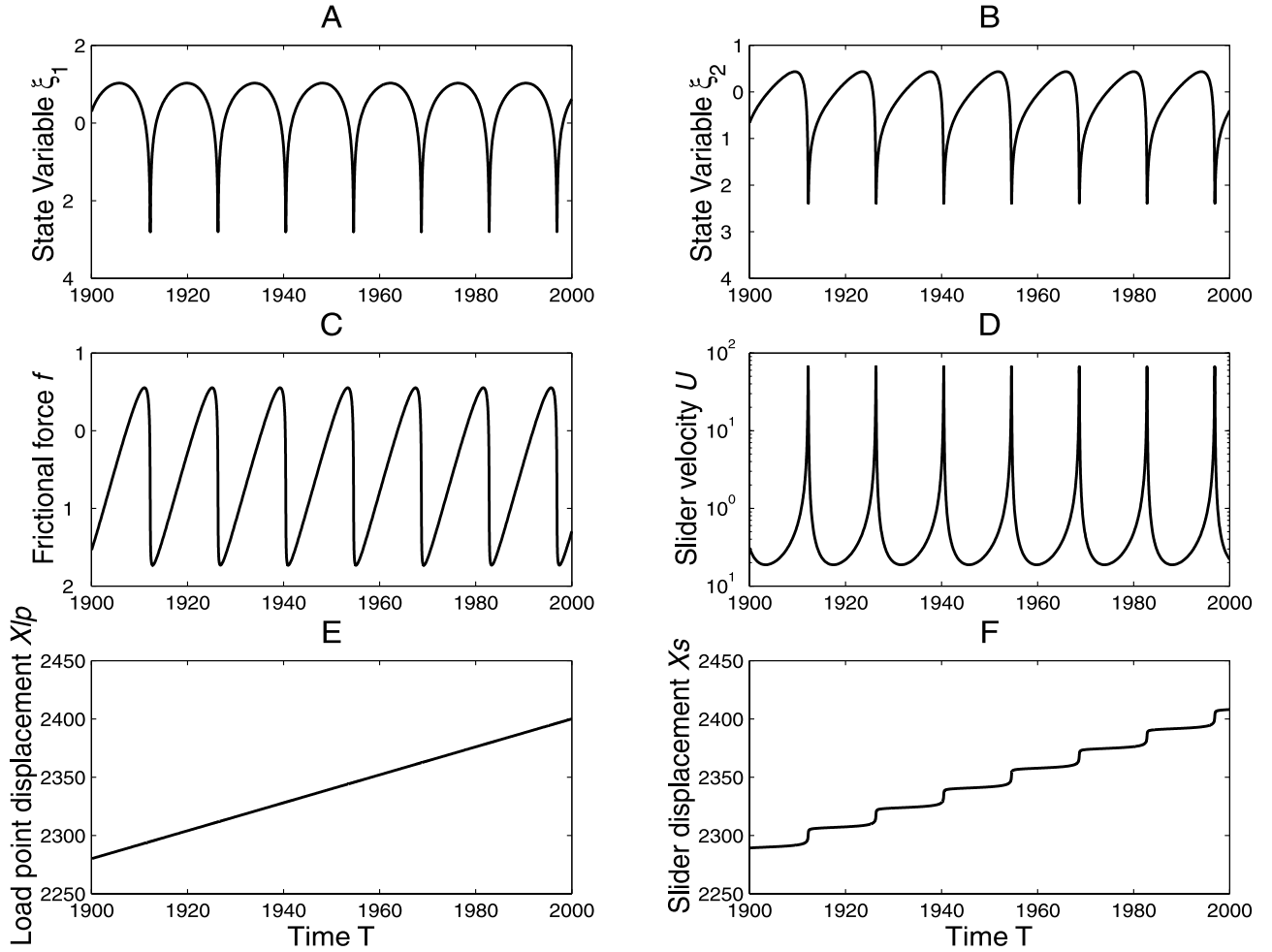


Figure 14. Temporal evolution of slider system for $k_* = 0.96$ with parameters $\beta_1 = 0.67$, $\beta_2 = 0.60$, $\rho = 0.27$, $M = 7.0 \times 10^{-17}$, and $U_b = 1.2$.

where A is the maximum amplitude of the sine wave, T_0^r is its period, N is the number of cycles and T_b^r is the time at which the transient is applied. By varying these four parameters, we can change the characteristics of the transient load, which often results in different responses of the slider system (We also tried using sine wave functions for displacement disturbance from the loading point, which corresponds to cosine wave transients for U_r . We found that the slider system displays similar responses as shown below).

[50] Figure 16 shows the evolution of the system after we apply a transient load at time $T_b^r = 1910$, when the slider velocity U is smaller than 1. The transient load is a single cycle ($N = 1$) sine wave with $A = 9.2 \times 10^4$ and $T_0^r = 1 \times 10^{-3}$. From Figures 16a and 16b, we can see that the next expected “creep event” is “clock advanced” and occurs shortly after the transient loading ends. Figure 16c is an zoom-in view of how the slider velocity U evolves during the transient loading. During the first half cycle of positive transient loading, the slider velocity increases with time. The velocity U , however, does not decrease immediately after the next half cycle is entered when the transient load becomes negative. Instead, it continues to increase to a maximum value before diminishing. Thus, at the end of the

cycle, the slider velocity achieves a much higher value compared with that at time T_b^r (just before the transient load is applied). This higher slider velocity U subsequently leads to an earlier occurrence of the anticipated creep event, which occurs shortly after the transient loading ends. Hence the effects of the positive and negative pulse of the symmetric sine wave do not cancel one another, instead the net result is to time advance the next creep event.

[51] Our numerical modeling reveals that the response of the system depends nonlinearly on the characteristics of transient loads. The “clock advance” effect is more prominent when a transient load with larger amplitude (A) and longer duration (larger N or T_0^r or both) is introduced late in the cycle of the creep events. When we decrease the amplitude A slightly from 9.2×10^4 , we find that the next anticipated creep event still can be “clock advanced” but with a longer time delay after the transient load stops. As the value of A decreases further, the “clock advance” effect becomes almost unobservable. Figures 17a and 17b demonstrate the response of the system after we halve the value of A to 4.6×10^4 . The timing of the next anticipated creep event is almost unaffected (Figure 17a). From Figure 17b we can still observe an increase in the slider velocity U during the first positive half cycle of transient loading and a

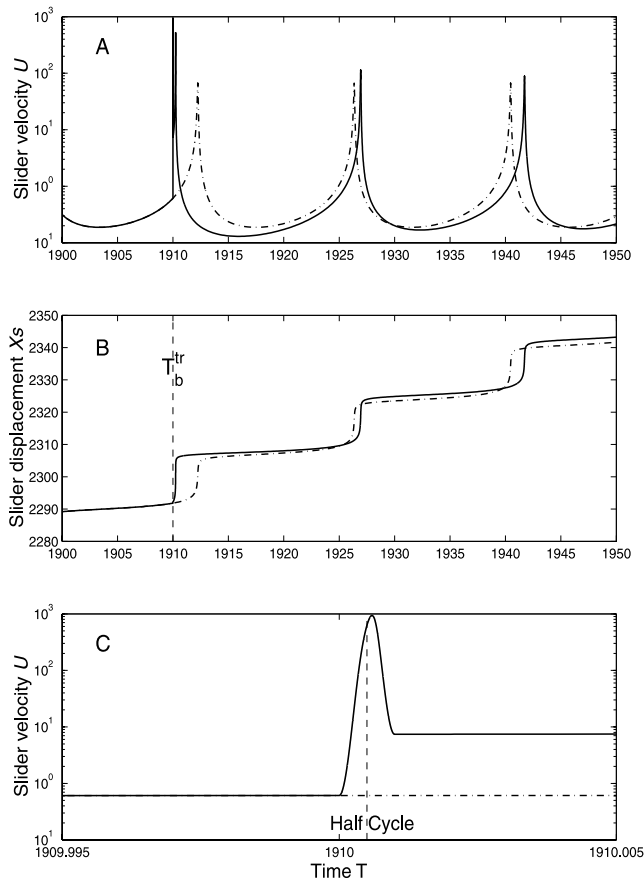


Figure 16. Comparison of slider behavior without (dash-dotted curve) and with (solid curve) the introduction of a transient load into the system. Sine wave transient load starts at time $T_b^{tr} = 1910$ with amplitude $A = 9.2 \times 10^4$, period $T_0^{tr} = 1 \times 10^{-3}$ and number of cycles $N = 1$. (a) Evolution of the slider velocity U , (b) Evolution of the slider displacement X_s , and (c) Zoom-in view of the change of slider velocity U during transient loading period.

greater number of cycles. When we change T_0^{tr} to 0.2×10^{-3} and N to 5, so that the new transient load has the same duration $N \times T_0^{tr} = 1 \times 10^{-3}$ and amplitude $A = 9.2 \times 10^4$ as the one in Figure 16, the timing of the next anticipated creep event is hardly affected. When we increase the amplitude A of the new transient with the shorter period, however, the “clock advance” effect becomes more prominent. Figures 17e and 17f show the evolution of the system after we increase A to 4.6×10^5 . We can see that the next anticipated creep event is triggered almost immediately by the transient load.

[54] Figure 18 shows the responses of the slider system to different transient loads with the same duration $N \times T_0^{tr} = 1 \times 10^{-3}$. Two thresholds of transient amplitude A exist and separate the responses of the slider system into three types. Above the upper limit dynamic events are triggered and below the lower one no triggering effect is observed. In between creep, events are time advanced. Our modeling also shows that the triggering effect is more prominent when transient loads are applied later in the cycle of creep events, i.e., when the preexisting slider velocity is higher.

[55] When we convert nondimensional time and velocity to dimensional ones using $U_* = 3 \times 10^{-10}$ m/s, $L_1 = 20 \mu\text{m}$

and $L_2 = 75 \mu\text{m}$ as before, we find that $A = 4.6 \times 10^5$ is equivalently to an amplitude of 1.38×10^{-4} m/s, $T_0^{tr} = 0.2 \times 10^{-3}$ corresponds to a period of 32 s and a duration $N \times T_0^{tr}$ of 160 s. These values are in the correct ranges for seismic waves produced by a $M \approx 6.0$ earthquake at distances of tens to several hundred kilometers. Hence, our modeling shows that certain transient loading with realistic characteristics may trigger creep events on a fault.

3.8. Discussion of Dynamic (Transient) Triggering

[56] The observation of widespread increases in seismicity (sometimes delayed) after the 1992 Landers earthquake, at distances where static Coulomb stress changes are negligible, led many researchers to consider the scenario of earthquake triggering by dynamic stresses. Debate, however, still exists on whether earthquakes can be triggered by the transient seismic waves generated by other events [Scholz, 1998; Gomberg *et al.*, 1998]. The numerical calculations by Cotton and Coutant [1997] showed that the dynamic stress changes associated with propagating waves fall off with radius less than r^{-1} . Instead, static changes in CFS have a fall of between r^{-2} and r^{-1} . Thus, at large distances from a main shock the value of dynamic stress changes can be an order of magnitude higher than those of static ones. This is the main reason why dynamic triggering is favored in explaining remotely triggered seismic events. Recently, the dynamic triggering hypothesis also was tested in the near field by researchers utilizing the directivity effect produced by large earthquakes, which can amplify shaking in the direction of earthquake rupture. Kilb *et al.* [2000] and Gomberg *et al.* [2001] found similar asymmetries in the aftershock and dynamic stress patterns from both the 1992 Mw 7.3 Landers and 1999 Mw 7.1 Hector Mine earthquakes. They also found that aftershocks are more likely to occur in areas of high dynamic shaking, as long as changes in static stress do not have the opposite effect and inhibit fault failure. Hence, they argued that dynamic stress changes can also promote fault failure close to an earthquake.

[57] In the same way that positive static stress changes can promote fault failure, negative ones can result in the formation of a stress shadow, where seismic activity is found to be suppressed for a period of time (see references in the study of Harris [1998]). Dynamic stress changes, however, are unlikely to explain such stress shadows since modeling shows that transient loads could not cause a time delay in the future instabilities [Gomberg *et al.*, 1997]. Marone [2000] suggests that one way to prove the role of dynamic triggering is to document a shaking-induced increase in seismic activity inside a static stress shadow.

[58] The modeling work of Gomberg *et al.* [1997] demonstrates that dynamic triggering of earthquakes is possible although they acknowledged that generation of clock advance of tens of days or more requires transient amplitudes that exceed those likely from seismic waves by about an order of magnitude. Our work shows that dynamic triggering of creep events is also possible under certain circumstances. Although we do not know the time history of dynamic loading on the faults that slipped after the 10 earthquakes in California, we can get a sense of the extent of ground shaking by examining intensity data at or near those places. We found that most of the slipped fault segments experienced a modified Mercalli intensity greater

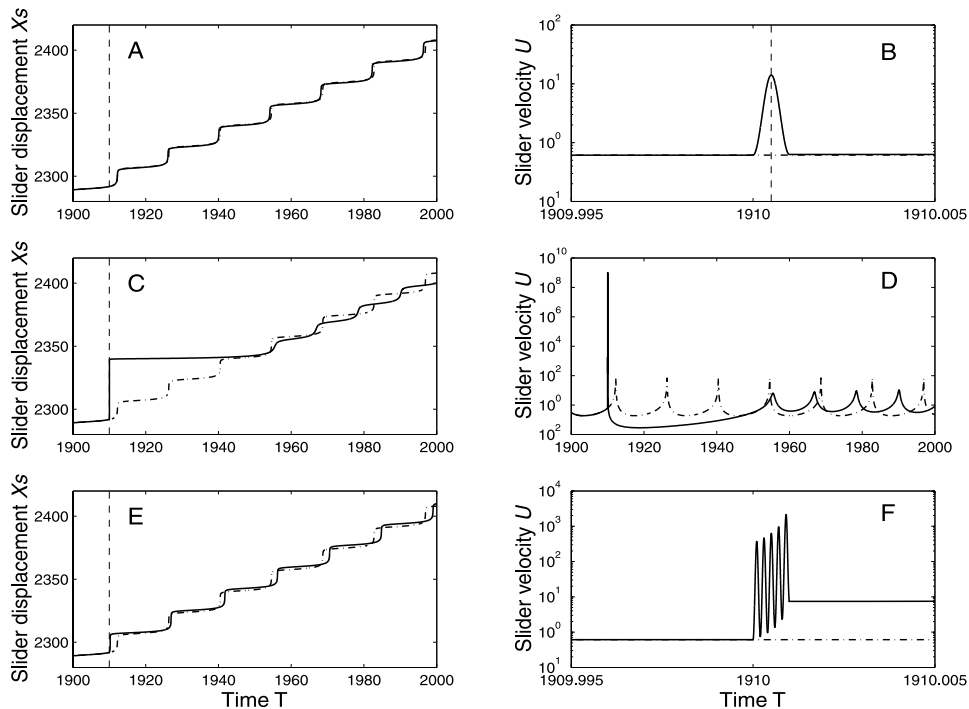


Figure 17. Evolution of the slider displacement X_s (a) and slider velocity U (b) after amplitude of sine wave transient load is halved to 4.6×10^4 . Evolution of the displacement X_s (c) and slider velocity U (d) after amplitude of sine wave transient load is elevated to 9.3×10^4 . Evolution of the displacement X_s (e) and slider velocity U (f) after period of sine wave transient is changed to 0.2×10^{-3} , the number of cycles N is enlarged to 5 and the amplitude A is increased to 4.6×10^5 . Slider behavior with only background loading is plotted with dash-dotted line, and those with the transient loading are shown by solid curves.

than or equal to V [Seismological Field Survey, NOAA, 1972; Reagor et al., 1982; Stover, 1984; McNutt and Topozada, 1990; Stover and Brewer, 1994]. Since the response of the slider system depends nonlinearly on the time the dynamic stress is applied in the creep cycle, which is equivalent to the preexisting condition on a fault right before the load is applied, and other characteristics of the transient loads, it is not easy to predict whether aseismic slip would be triggered on a fault if a nearby earthquake occurs.

[59] Unlike the static Coulomb stress model used in evaluating the static triggering scenario, which incorporates the contribution from the changes in normal stress, we assume constant normal stress in our numerical modeling of transient loading upon creep events. Linker and Dieterich [1992] and Richardson and Marone [1999] studied the effect of changing normal stress for the one-state-variable frictional law. Recently, Perfettini and Schmittbuhl [2001] and Perfettini et al. [2001] examined the effect of time-varying normal and shear stress perturbations on a creeping fault. They interpreted some of their modeling results in terms of earthquake triggering by Earth tides. We think that including time-varying normal stress would lead to a better understanding of the impact of transient loading on aseismic fault slip, although the main results from this study would not be affected.

4. Conclusion

[60] We study the phenomenon of “triggered aseismic slip” on nearby faults by moderate to large earthquakes.

The possible triggering role of static stress changes is evaluated by examining observations made after 10 events in California using a static Coulomb stress model. Most of the fault segments that slipped aseismically experienced positive changes in static CFS associated with nearby shocks. Some of those positive values, however, are very small. Also, three discrepancies or failures of the hypothesis of triggering slow slip exist for a segment of the southern San Andreas fault after the 1987 Elmore Ranch and Superstition Hills earthquake sequence and a segment of the southern Calaveras fault after the 1989 Loma Prieta shock. Hence, we conclude that static stress triggering either is not or is not the sole mechanism responsible for the observed triggered slip.

[61] We then use a spring-slider system as a very simple fault model to study its slip behavior and its response to dynamic stress loading. When a two-state-variable rate-dependent and state-dependent frictional law is used, creep events are modeled in a velocity-weakening regime with system stiffness smaller than but close to a critical value. Thus, when applied to real crustal faults, our work results in a two-layer model for fault creep phenomenon similar to that proposed by Bilham and Behr [1992]. Above a transition depth the fault slides in a stable fashion (i.e., it undergoes secular creep) in both the velocity-strengthening and the conditionally stable regimes. Our modeled creep events (or episodic creep) originate in a layer below that depth but above the seismogenic layer where earthquakes nucleate. They may propagate into the two regions above from their nucleation zone. Similar creep events also may

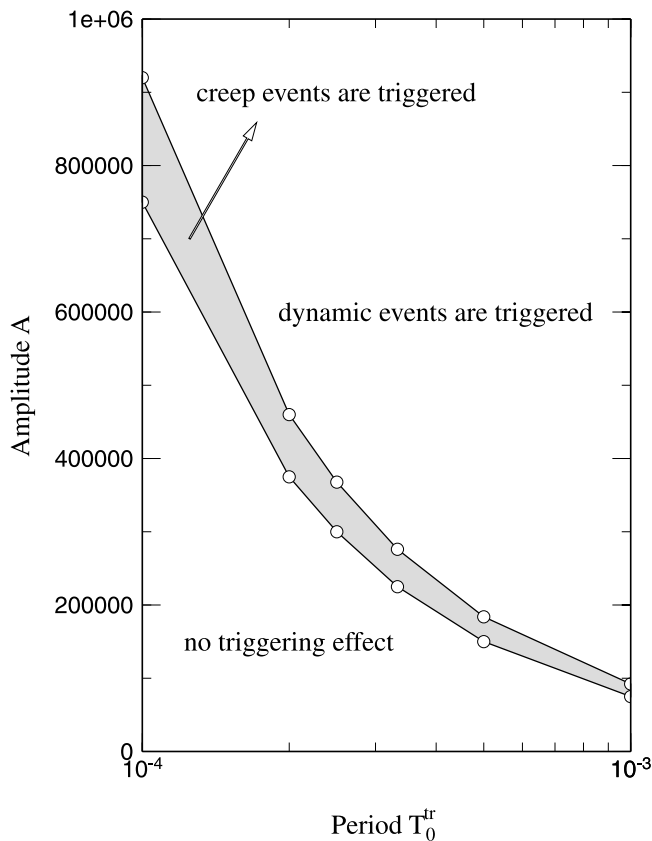


Figure 18. Responses of slider system to different transient loads with the same durations $N \times T_0^{\text{tr}} = 1 \times 10^{-3}$. Shaded region is where creep events are triggered. Dynamic events like those in Figures 17c and 17d are triggered instead above that region, while no triggering effect is observed below it.

occur at the base of the seismogenic zone. We use a sine wave transient (dynamic) load to simulate the passage of waves radiated by a nearby earthquake and apply it as a forcing function to the spring-slider system. Our numerical modeling reveals that the response of the system depends nonlinearly on the characteristics of transient loads, such as amplitude, period, number of cycles and applied time. We find that certain types of transient loads can cause a large time advance of (or trigger) the next anticipated creep events, which then occur either shortly after the transient load ends or with a time delay.

[62] While our work examines triggered creep events near the surface, it may well have implications for the occurrence of similar events near the bottom of the seismogenic zone of faults where a transition occurs from velocity-weakening to velocity-strengthening behavior. Creep events, including slow earthquakes, near that transition may be common on timescale of days to months. Relatively little data exist, however, on whether they occur often or rarely. If they occur frequently, they may load the shallower, velocity-weakening parts of faults and sometimes trigger the occurrence of moderate to large earthquakes.

[63] **Acknowledgments.** We acknowledge the helpful comments by M. Cocco and two anonymous reviewers. We would also thank T. Tullis and D. Schaff for their comments on the manuscript. The stress field was

calculated using DIS3D program, which was originally written by S. Dunbar and later improved by Erickson [1986] using the expressions of G. Converse. This study was supported by Southern California Earthquake Center (SCEC) grant USCPO 569934. SCEC is funded by NSF Cooperative Agreement EAR-8920136 and USGS Cooperative Agreements 14-08-0001-A0899 and 1434-HQ-97AG01718. This is SCEC publication 699 and Lamont-Doherty Earth Observatory contribution LDEO 6386.

References

- Allen, C. R., M. Wyss, J. N. Brune, A. Granz, and R. Wallace, Displacements on the Imperial, Superstition Hills, and San Andreas faults triggered by the Borrego Mountain Earthquake, in *The Borrego Mountain Earthquake, U.S. Geol. Surv. Prof. Pap.*, vol. 787, pp. 87–104, 1972.
- Anderson, G., and H. Johnson, A new statistical test for static stress triggering: Application to the 1987 Superstition Hills earthquake sequence, *J. Geophys. Res.*, *104*, 20,153–20,168, 1999.
- Anderson, J. G., J. N. Brune, J. N. Louie, Y. Zeng, M. Savage, G. Yu, Q. Chen, and D. dePollo, Seismicity in the western Great Basin apparently triggered by the Landers, California, earthquake, 28 June 1992, *Bull. Seismol. Soc. Am.*, *84*, 863–891, 1994.
- Archuleta, R. J., A faulting model for the 1979 Imperial Valley earthquake, *J. Geophys. Res.*, *89*, 4559–4585, 1984.
- Beeler, N. M., R. W. Simpson, S. H. Hickman, and D. A. Lockner, Pore fluid pressure, apparent friction, and Coulomb failure, *J. Geophys. Res.*, *105*, 25,533–25,542, 2000.
- Belardinelli, M. E., Increase of creep interevent intervals: A conceptual model, *Tectonophysics*, *277*, 99–107, 1997.
- Belardinelli, M. E., M. Cocco, O. Coutant, and F. Cotton, Redistribution of dynamic stress during coseismic ruptures: Evidence for fault interaction and earthquake triggering, *J. Geophys. Res.*, *104*, 14,925–14,945, 1999.
- Bilham, R., and J. Behr, A two-layer model for aseismic slip on the Superstition Hills fault, California, *Bull. Seismol. Soc. Am.*, *82*, 1223–1235, 1992.
- Boatwright, J., and M. Cocco, Frictional constraints on crustal faulting, *J. Geophys. Res.*, *101*, 13,895–13,909, 1996.
- Bodin, P., R. Bilham, J. Behr, J. S. Gombert, and K. W. Hudnut, Slip triggered on Southern California faults by the 1992 Joshua Tree, Landers, and Big Bear earthquakes, *Bull. Seismol. Soc. Am.*, *84*, 806–816, 1994.
- Brace, W. F., and J. D. Byerlee, Stick-slip as a mechanism for earthquakes, *Science*, *153*, 990–992, 1966.
- Burdick, L. J., and G. R. Mellman, Inversion of the body waves from the Borrego Mountain earthquake to the source mechanism, *Bull. Seismol. Soc. Am.*, *66*, 1485–1499, 1976.
- Cocco, M., and J. R. Rice, Pore pressure and poroelasticity effects in Coulomb stress analysis of earthquake interactions, *J. Geophys. Res.*, *107*, doi:10.1029/2000JB000138, 2002.
- Cotton, F., and O. Coutant, Dynamic stress variations due to shear faults in a plane-layered medium, *Geophys. J. Int.*, *128*, 676–688, 1997.
- Dieterich, J. H., Time dependent friction and the mechanics of stick slip, *Pure Appl. Geophys.*, *116*, 790–806, 1978.
- Dieterich, J. H., Modeling of rock friction 1. Experimental results and constitutive equations, *J. Geophys. Res.*, *84*, 2161–2168, 1979.
- Dieterich, J. H., Constitutive properties of faults with simulated gouge, in *Mechanical Behavior of Crustal Rocks, Geophys. Monogr. Ser.*, vol. 24, edited by N. L. Carter et al., pp. 103–120, Washington, D. C., 1981.
- Ebel, J. E., and D. V. Helmberger, P-wave complexity and fault asperities: The Borrego Mountain, California, earthquake of 1968, *Bull. Seismol. Soc. Am.*, *72*, 413–438, 1982.
- Erickson, L., User's manual for DIS3D: A three-dimensional dislocation program with applications to faulting in the earth, M.S. thesis, Stanford Univ., Stanford, Calif., 1986.
- Fuis, G. S., Displacement on the Superstition Hills fault triggered by the earthquake, in *The Imperial Valley Earthquake of October, 15, 1979, U.S. Geol. Surv. Prof. Pap.*, vol. 1254, pp. 145–154, 1982.
- Galehouse, J. S., Effect of the Loma Prieta earthquake on surface slip along the Calaveras fault in the Hollister area, *Geophys. Res. Lett.*, *17*, 2019–2022, 1990.
- Gombert, J. S., Stress/strain changes and triggered seismicity following the Mw7.3 Landers, California, earthquake, *J. Geophys. Res.*, *101*, 751–764, 1996.
- Gombert, J. S., and P. Bodin, Triggering of the Ms = 5.4 Little Skull Mountain, Nevada Earthquake with Dynamic strains, *Bull. Seismol. Soc. Am.*, *84*, 844–853, 1994.
- Gombert, J. S., M. L. Blanpied, and N. M. Beeler, Transient triggering of near and distant earthquakes, *Bull. Seismol. Soc. Am.*, *87*, 294–309, 1997.
- Gombert, J. S., N. M. Beeler, M. L. Blanpied, and P. Bodin, Earthquake triggering by transient and static deformation, *J. Geophys. Res.*, *103*, 24,411–24,426, 1998.

- Gomberg, J. S., P. A. Reasenberg, P. Bodin, and R. A. Harris, Earthquake triggering by seismic waves following the Landers and Hector Mine earthquakes, *Nature*, 411, 462–466, 2001.
- Gouly, N. R., and R. Gilman, Repeated creep events on the San Andreas fault near Parkfield, California, recorded by a strainmeter array, *J. Geophys. Res.*, 83, 5415–5419, 1978.
- Gu, Y., and T. F. Wong, Effects of loading velocity, stiffness, and inertia on the dynamics of a single degree of freedom spring-slider system, *J. Geophys. Res.*, 96, 21,677–21,691, 1991.
- Gu, J. C., J. R. Rice, A. L. Ruina, and S. T. Tse, Slip motion and stability of a single degree of freedom elastic system with rate and state dependent friction, *J. Mech. Phys. Solids*, 32, 167–196, 1984.
- Hamilton, R. M., Aftershocks of the Borrego Mountain earthquake from April 12 to June 12, 1968, *U.S. Geol. Surv. Prof. Pap.*, 787, 31–54, 1972.
- Harris, R. A., Introduction to special section: Stress triggers, stress shadows, and implications for seismic hazard, *J. Geophys. Res.*, 103, 24,347–24,358, 1998.
- Hill, D. P., et al., Earthquakes remotely triggered by the magnitude 7.3 Landers, California, seismicity, *Science*, 260, 1617–1623, 1993.
- Hudnut, K. W., and M. M. Clark, New slip along parts of the 1968 Coyote Creek fault rupture, California, *Bull. Seismol. Soc. Am.*, 79, 451–465, 1989.
- Ida, Y., Slow moving deformation pulses along tectonic faults, *Phys. Earth Planet. Inter.*, 9, 328–337, 1974.
- Kikuchi, M., and H. Kanamori, Inversion of complex body waves, 2, *Phys. Earth Planet. Inter.*, 43, 205–222, 1985.
- Kilb, D., J. Gomberg, and P. Bodin, Triggering of earthquake aftershocks by dynamic stresses, *Nature*, 408, 570–574, 2000.
- King, G. C. P., and M. Cocco, Fault interaction by elastic stress changes: New clues from earthquake sequences, *Adv. Geophys.*, 44, 1–38, 2001.
- Lienkaemper, J. J., J. S. Galehouse, and R. W. Simpson, Creep response of the Hayward fault to stress changes caused by the Loma Prieta earthquake, *Science*, 276, 2014–2016, 1997.
- Linde, A. T., M. T. Gladwin, M. J. S. Johnston, R. L. Gwyther, and R. G. Bilham, A slow earthquake sequence on the San Andreas fault, *Nature*, 383, 65–68, 1996.
- Linker, M. F., and J. H. Dieterich, Effects of variable normal stress on rock friction: Observations and constitutive equations, *J. Geophys. Res.*, 97, 4923–4940, 1992.
- Lisowski, M., W. H. Prescott, J. C. Savage, and M. J. Johnson, Geodetic estimate of coseismic slip during the 1989 Loma Prieta, California, earthquake, *Geophys. Res. Lett.*, 17, 1437–1440, 1990.
- Louie, J. N., C. R. Allen, D. C. Johnson, P. C. Haase, and S. N. Cohn, Fault slip in southern California, *Bull. Seismol. Soc. Am.*, 75, 811–833, 1985.
- Marone, C. J., C. H. Scholz, and R. Bilham, On the mechanics of earthquake afterslip, *J. Geophys. Res.*, 96, 8441–8452, 1991.
- Marone, C. J., Shaking faults loose, *Nature*, 408, 534–535, 2000.
- Mavko, G. M., S. S. Schulz, and B. D. Brown, Effects of the 1983 Coalinga, California, earthquake on creep along the San Andreas fault, *Bull. Seismol. Soc. Am.*, 75, 475–489, 1985.
- McClellan, P. H., and E. A. Hay, Triggered slip on the Calaveras fault during the magnitude 7.1 Loma Prieta earthquake, *Geophys. Res. Lett.*, 17, 1227–1230, 1990.
- McGill, S. F., C. R. Allen, K. W. Hudnut, D. C. Johnson, W. F. Miller, and K. E. Sieh, Slip on the Superstition Hills fault and on nearby faults associated with the 24 November 1987 Elmore Ranch and Superstition Hills earthquakes, southern California, *Bull. Seismol. Soc. Am.*, 79, 362–375, 1989.
- McNutt, S. R., and T. R. Toppozada, Seismological Aspects of the 17 October 1989 earthquake, in *The Loma Prieta (Santa Cruz Mountains), California, Earthquake of 17 October 1989, Div. Mines Geol., Spec. Publ.*, vol. 104, edited by S. R. McNutt and R. H. Sydner, pp. 11–27, 1990.
- Melchior, P. J., *The Tides of the Planet Earth*, 2nd ed., 641 pp., Pergamon, New York, 1983.
- Miller, M. M., T. Melbourne, D. J. Johnson, and W. Q. Sumner, Periodic slow earthquakes from the Cascadia subduction zone, *Science*, 295, 2423, 2002.
- Nalbant, S. S., A. Hubert, and G. C. P. King, Stress coupling between earthquakes in northwest Turkey and the north Aegean Sea, *J. Geophys. Res.*, 103, 24,469–24,486, 1998.
- Nason, R. D., Investigation of fault slippage in northern and central California, Ph.D. thesis, 231 pp., Univ of Calif., San Diego, 1971.
- Nason, R. D., and J. Weertman, A dislocation theory analysis of fault creep events, *J. Geophys. Res.*, 78, 7745–7751, 1973.
- Okada, Y., Internal deformation due to shear and tensile faults in a half-space, *Bull. Seismol. Soc. Am.*, 82, 1018–1040, 1992.
- Perfettini, H., and J. Schmittbuhl, Periodic loading on a creeping fault: Implications for tides, *Geophys. Res. Lett.*, 28, 435–438, 2001.
- Perfettini, H., J. Schmittbuhl, J. R. Rice, and M. Cocco, Frictional response induced by time-dependent fluctuations of the normal loading, *J. Geophys. Res.*, 106, 13,455–13,472, 2001.
- Petersen, M. D., L. Seeber, L. R. Sykes, J. L. Nábelek, J. G. Armbruster, J. Pacheco, and K. W. Hudnut, Seismicity and fault interaction, southern San Jacinto fault zone and adjacent faults, southern California: Implications for seismic hazard, *Tectonics*, 10, 1187–1203, 1991.
- Press, W. H., S. A. Teukolsky, W. T. Vetterling, and B. P. Flannery, *Numerical Recipes in C, The Art of Scientific Computing*, second edition, Cambridge Univ. Press, New York, 1992.
- Reagor, B. G., C. W. Stover, S. T. Algermissen, K. V. Steinbrugge, P. Hubiak, M. G. Hopper, and L. M. Barnhard, Preliminary evaluation of the distribution of seismic intensities, in *The Imperial Valley Earthquake of October 15, 1979, U.S. Geol. Surv. Prof. Pap.*, vol. 1254, pp. 251–258, 1982.
- Rice, J. R., and A. L. Ruina, Stability of steady frictional slipping, *J. Appl. Mech.*, 105, 343–349, 1983.
- Rice, J. R., and S. T. Tse, Dynamic motion of a single degree of freedom system following a rate and state dependent friction law, *J. Geophys. Res.*, 91, 521–530, 1986.
- Richardson, E., and C. J. Marone, Effects of normal stress vibrations on frictional healing, *J. Geophys. Res.*, 104, 28,859–28,878, 1999.
- Roy, M., and C. Marone, Earthquake nucleation on model faults with rate- and state-dependent friction: Effects of inertia, *J. Geophys. Res.*, 101, 13,919–13,932, 1996.
- Ruina, A. L., Friction laws and instabilities: A quasistatic analysis of some dry frictional behavior, Ph.D. thesis, Brown Univ., Providence, R. I., 1980.
- Ruina, A. L., Slip instability and state variable friction laws, *J. Geophys. Res.*, 88, 10,359–10,370, 1983.
- Scholz, C. H., *The Mechanics of Earthquakes and Faulting*, Cambridge Univ. Press, New York, 1990.
- Scholz, C. H., Earthquake and friction laws, *Nature*, 391, 37–41, 1998.
- Scholz, C. H., P. Molnar, and T. Johnson, Detailed studies of frictional sliding of granite and implications for the earthquake mechanism, *J. Geophys. Res.*, 77, 6393–6406, 1972.
- Schulz, S. S., G. M. Mavko, R. O. Burford, and W. D. Stuart, Long-term fault creep observations in central California, *J. Geophys. Res.*, 87, 6977–6982, 1982.
- Seismological Field Survey, NOAA, Intensity distribution and field effects, strong-motion seismograph records, and response spectra, in *The Borrego Mountain Earthquake, U.S. Geol. Surv. Prof. Pap.*, vol. 787, pp. 141–157, 1972.
- Sharp, R. V., Pre-earthquake displacement and triggered displacement on the Imperial fault associated with the Superstition Hills earthquake of 24 November 1987, *Bull. Seismol. Soc. Am.*, 79, 466–479, 1989.
- Sharp, R. V., M. J. Rymer, and J. J. Lienkaemper, Surface displacements on the Imperial and Superstition Hills faults triggered by the Westmorland, California, earthquake of 26 April 1981, *Bull. Seismol. Soc. Am.*, 76, 1838–1843, 1986a.
- Sharp, R. V., M. J. Rymer, and D. M. Morton, Trace-fractures on the Banning fault created in association with the 986 North Palm Springs earthquake, *Bull. Seismol. Soc. Am.*, 76, 1838–1843, 1986b.
- Sieh, K. E., Slip along the San Andreas associated with the earthquake, in *The Imperial Valley Earthquake of October 15, 1979, U.S. Geol. Surv. Prof. Pap.*, vol. 1254, pp. 155–160, 1982.
- Simpson, R. W., and P. A. Reasenberg, Earthquake-induced static stress changes on central California faults, in *The Loma Prieta, California, Earthquake of October 17, 1989: Earthquake Occurrence: Tectonic Processes and Models, U.S. Geol. Surv. Prof. Pap.*, vol. 1550-F, pp. F55–F89, 1994.
- Simpson, R. W., S. S. Schulz, L. D. Dietz, and R. O. Burford, The response of creeping parts of the San Andreas fault to earthquakes on nearby faults: Two examples, *Pure Appl. Geophys.*, 126, 665–685, 1988.
- Steinbrugge, K. V., and E. G. Zacher, Creep on the San Andreas fault: Fault creep and property damage, *Bull. Seismol. Soc. Am.*, 50, 389–396, 1960.
- Steketee, J. A., On Volterra's dislocations in a semi-infinite elastic medium, *Can. J. Phys.*, 36, 192–205, 1958.
- Stein, R. S., The role of stress transfer in earthquake occurrence, *Nature*, 402, 605–609, 1999.
- Stesky, R. M., Mechanisms of high temperature frictional sliding in Westerly granite, *Can. J. Earth Sci.*, 15, 361–375, 1978.
- Stover, C. W., *United States Earthquakes, 1981*, pp. 21–26, U.S. Dept. of the Interior, USGS, Washington, D. C., 1984.
- Stover, C. W., and L. R. Brewer, *United States Earthquakes, 1986*, pp. 32–41, U.S. Dept. of the Interior, USGS, Washington, D. C., 1994.
- Stuart, W. D., R. J. Archuleta, and A. G. Lindh, Forecast model for moderate earthquakes near Parkfield, *J. Geophys. Res.*, 90, 592–604, 1985.
- Sylvester, A. G., Near-field tectonic geodesy, in *Active Tectonics*, pp. 164–180, Natl. Acad. Press, Washington, D. C., 1986.

- Tocher, D., Creep on the San Andreas fault: Creep rate and related measurements at Vineyard, California, *Bull. Seismol. Soc. Am.*, *50*, 396–404, 1960.
- Tse, S. T., and J. R. Rice, Crustal earthquake instability in relation to the depth variation of frictional slip properties, *J. Geophys. Res.*, *91*, 9452–9472, 1986.
- Wesson, R. L., Dynamics of fault creep, *J. Geophys. Res.*, *93*, 8929–8951, 1988.
- Williams, P. L., S. F. McGill, K. E. Sieh, C. R. Allen, and J. N. Louie, Triggered slip along the San Andreas fault after the 8 July 1986 North Palm Springs earthquake, *Bull. Seismol. Soc. Am.*, *78*, 1112–1122, 1988.
- Ziv, A., and A. M. Rubin, Static stress transfer and earthquake triggering: No lower threshold in sight?, *J. Geophys. Res.*, *105*, 13,631–13,642, 2000.
-
- W.-x. Du, Department of Geology and Geophysics, University of Wisconsin-Madison, 1215 W. Dayton St., Madison, WI 53706, USA. (dxw@geology.wisc.edu)
- C. H. Scholz, B. E. Shaw, and L. R. Sykes, Lamont-Doherty Earth Observatory, Columbia University, PO Box 1000, Palisades, NY 10964, USA.